Received: 26 July 2023 | Revised: 24 October 2023 | Accepted: 12 November 2023

DOI: 10.1111/bre.12834

Basin Research IAS EAGE WILEY

RESEARCH ARTICLE

Early Jurassic initiation of the modern drainage pattern of the Dabie orogen (East China) revealed by a multi-proxy provenance approach

Tao Deng[1] | **Xiumian Hu**[1] | **David Chew**[2] | **Jan Schönig**[3] | **Anlin Ma**[1] | **Wendong Liang**[4] | **Foteini Drakou**[2]

[1]State Key Laboratory of Mineral Deposit Research, School of Earth Sciences and Engineering, Nanjing University, Nanjing, China

[2]Department of Geology, School of Natural Sciences, Trinity College Dublin, Dublin, Ireland

[3]Department of Sedimentology and Environmental Geology, Geoscience Center, University of Göttingen, Göttingen, Germany

[4]State Key Laboratory of Oil and Gas Reservoir Geology and Exploitation, Institute of Sedimentary Geology, Chengdu University of Technology, Chengdu, China

Correspondence
Xiumian Hu, State Key Laboratory of Mineral Deposit Research, School of Earth Sciences and Engineering, Nanjing University, Nanjing 210029, China.
Email: huxm@nju.edu.cn

Funding information
National Natural Science Foundation of China, Grant/Award Number: 42050102 and 41888101; Science Foundation Ireland (SFI), Grant/Award Number: 12/IP/1663, 13/RC/2092, 13/RC/2092_P2 and 15/IA/3024

Abstract

The timing of the initiation of the present-day tectonic architecture and drainage systems in eastern China remains debated. This study presents a comprehensive provenance study of the Early Jurassic peripheral basins surrounding the Dabie orogen including framework petrography, heavy-mineral analysis, single-grain chronology and chemistry. Clasts of high-grade schist, muscovite grains, rare gneissic fragments, abundant metamorphic garnet and phengite (Si > 3.3 pfu), combined with a main 216–256 Ma rutile U–Pb population found in these Early Jurassic sandstones, indicate a source from the Triassic (U)HP belt in the Dabie orogen. Sedimentary lithics and ultra-stable heavy-mineral assemblages indicate an additional source of recycled sedimentary rocks. Combined with the continuous shift of the youngest detrital rutile age population toward younger ages toward the north that mimics the pattern of metamorphic bedrock ages in the Dabie orogen, we infer that the present surface tectonic architecture and paleodrainage patterns of the Dabie orogen were established in the Early Jurassic. Thus, the Early Jurassic exhumation of the Dabie orogen marked the development of the watershed between Northern and Southern China, namely the Huai River and several principal tributary systems of the middle-lower Yangtze River.

KEYWORDS

Dabie orogen, drainage pattern, multi-mineral U–Pb geochronology, provenance analysis, UHP exhumation

1 | INTRODUCTION

The Dabie-Sulu orogen is one of the largest ultrahigh-pressure (UHP) metamorphic belts on Earth. Today, the Qinling-Dabie orogen defines a sharp break between North and South China in terms of tectonics, drainage patterns, landforms and climate (Figure 1a,b). It is generally regarded to have formed in the Triassic by the deep subduction of the South China Block (SCB) beneath the North China Craton (NCC) and

subsequent continental collision (Zhang et al., 2009; Zheng et al., 2019). The presence of coesite (Wang et al., 1989), microdiamonds (Xu et al., 1992), and the exsolution of clinopyroxene, rutile and apatite in garnet within the eclogites (Okay et al., 1989; Ye, Cong, & Ye, 2000), gneisses (Liu et al., 2001; Ye, Yao, et al., 2000) and marbles (Liu et al., 2006) in the Dabie-Sulu orogen demonstrate that the crustal rocks were once subducted to mantle depths greater than 200 km and subsequently exhumed to Earth's surface. Previous studies have constrained the spatial distribution of the HP-UHP belt, the timing of metamorphism and the mechanism(s) responsible for the exhumation of UHP rocks (see the review of Zheng et al., 2019). In contrast, the onset of exhumation as well as the timing of exposure of the UHP terrane on Earth's surface are less well-constrained and controversial yet are important to understand the late stages of its orogenic evolution. The timing of initial Triassic HP-UHP exhumation to the Earth's surface is only broadly constrained, ranging from the Middle-Late Triassic (ca. 240–220 Ma, Zhu et al., 2006), Early Jurassic (ca. 190 Ma, Wang et al., 2009; Zhang et al., 2017) to the Middle Jurassic (190–160 Ma, Grimmer et al., 2003; Yang et al., 2010). Therefore, tracing the uplift and denudation history of the Dabie orogen can potentially constrain the earliest development of the watershed between northern and southern China, between the Yangtze River and the Huai River basins (Figure 1a,b).

Basin sediments represent eroded and transported material from source region(s) at the time of deposition, which in many cases are orogenic belts. Hence, the sedimentary record represents a key archive for constraining exhumation and erosion histories. The HP-UHP metamorphic rocks of the Dabie orogen are presently exposed over a large region and investigating the sedimentary provenance in proximal sedimentary basins is an effective tool to constrain the exhumation and denudation processes within an orogen. Single-grain information in sedimentary records is widely used to trace the exhumation of UHP metamorphic rocks in orogenic belts (Canil et al., 2006). These lines of evidence include (1) coesite, diamond, pyrope, omphacite and high-Si phengite UHP inclusions in refractory detrital minerals such as garnet, zircon and rutile (Baldwin et al., 2021; Chen et al., 2005; Hart et al., 2016; Li et al., 2005; Schönig et al., 2018, 2019, 2022); (2) the occurrence of eclogite-facies metamorphic zircon with low Th/U ratios (<0.1), HREE depletion and an absent or minor negative Eu anomaly (Li et al., 2005; Rubatto, 2017; Zhang et al., 2022); and (3) the occurrence of eclogite-facies metamorphic garnet (especially the pyrope end-member), omphacite (jadeite) and phengite (especially Si > 3.5 atoms per formula unit [pfu; O = 11]) (Grimmer et al., 2003). Early-Middle Jurassic sedimentary basins around the Dabie orogen include the Hefei, Nanjing, Yueshan and Huangshi basins, which are immediately north, northeast, east and south of the Dabie orogen, respectively (Figure 1d). These basins preserve a unique record of the exhumation and unroofing history of the Dabie orogen.

Highlights

- The present drainage pattern of the Dabie orogen was established in the Early Jurassic.
- The Triassic HP-UHP rocks in the Dabie orogen were exposed to the Earth's surface by the Early Jurassic.
- A proposed Early Jurassic 2000-km-long and west-draining transcontinental river system in eastern China is challenged.

It is generally agreed that the provenance of the Early Jurassic strata of the Hefei basin to the north of the Dabie orogen is derived from the exhumation of Dabie Triassic HP-UHP rocks. Evidence includes the occurrence of pyrope-rich garnet grains and Middle-Late Triassic eclogite-facies metamorphic zircons, some of which contain coesite inclusions (Chen et al., 2005; Li et al., 2005). However, the source of a major 1.8 Ga zircon population in the basal Fanghushan Formation in the Hefei basin is debated, with contrasting interpretations regarding the source including the NCC and the Dabie orogen (Li et al., 2005; Wang et al., 2020). This has hindered the reconstruction of the paleodrainage patterns and the unroofing history of the Dabie orogen. The provenance of the Lower Jurassic sandstones in the Yueshan and Huangshi basins on the east and south side of the Dabie orogen is also contentious with different models being proposed. She et al. (2012) and Yang et al. (2010) argue for a source in the Wuyi terrane of the Cathaysia Block in the SCB (located southeast of the Yueshan and Huangshi basins) based on the presence of major Paleoproterozoic 1.8 Ga detrital zircon populations in these Lower Jurassic quartz sandstones and palaeocurrent data suggesting transport to the west. These constraints have been used to suggest the existence of a ca. 2000 km long, west-flowing transcontinental palaeo-river with an absence of material shed from the Dabie orogen. Similarly, Li, Li, Sun, and Zhang (2003), Li, Li, Zheng, et al. (2003) preclude a Late Triassic syn-orogenic contribution from the Dabie orogen to the sediments of the Huangshi basin based on sandstone compositions, and conclude that a Dabie orogen provenance is first seen in the Middle Jurassic successions of the Huangshi basin. In contrast, based

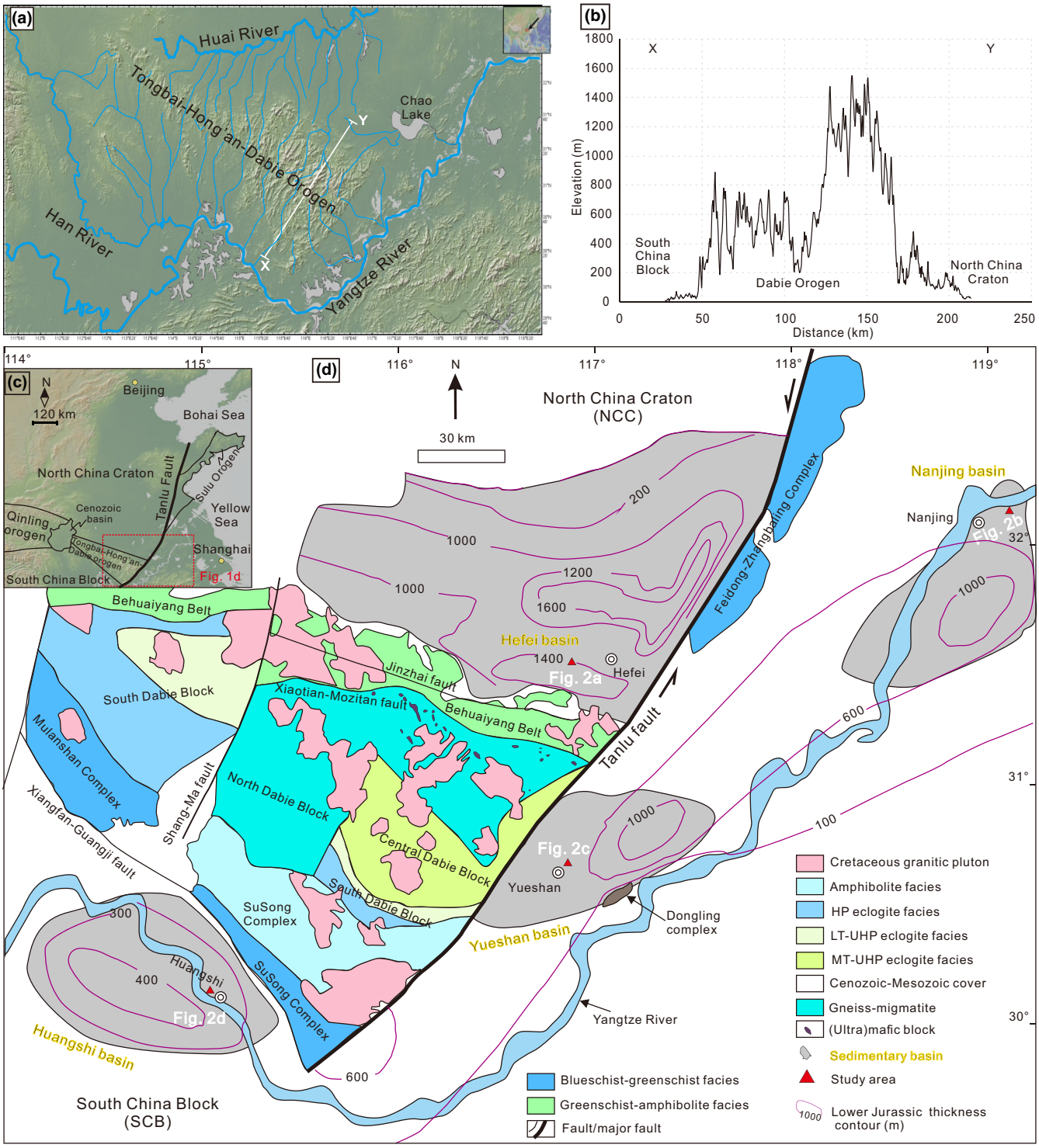

FIGURE 1 Hydrologic, geographic and geologic overview of the Tongbai-Hong'an-Dabie-Sulu orogen. (a) Modern topographic relief and major rivers of East Asia, with the present-day drainage pattern in eastern China illustrated. (b) Topography across the Dabie orogen (X-Y profile). (c) Simplified structural map showing the tectonic divisions of the Tongbai-Hong'an-Dabie-Sulu orogen; (d) Simplified geological map of the Dabie orogen and Jurassic sedimentary basins (after Hacker et al., 2000; Ratschbacher et al., 2000; Zheng et al., 2019). Isopachs of the Lower Jurassic deposits (m) are from Zhu et al. (2009).

on phengite (Si > 3.3 pfu) $^{40}Ar/^{39}Ar$ Triassic ages in the Lower Jurassic strata of the Huangshi and Yueshan basins, Grimmer et al. (2003) and Wang et al. (2009) emphasise a partial contribution from the Dabie orogen. Finally, studies on the provenance of the Lower Jurassic sequences in the Nanjing basin to the northeast of the Dabie orogen are rare. Based on two detrital zircon samples, Li and Hu (2022) inferred that the provenance of

the Lower Jurassic in the Nanjing basin was the result of a mixed contribution from the NCC and the SCB, but the potential involvement of the Dabie orogen remains elusive.

Thus, the inconsistency between the multiple proposed paleodrainage models hampers the reconstruction of the evolution of the drainage pattern of the Dabie orogen, with open questions including (1) whether these syn-orogenic Lower Jurassic sedimentary basins record a Dabie orogen provenance, and (2) when the Triassic HP-UHP rocks were first exposed on the surface.

In this paper, we investigate the evolution of Lower Jurassic sedimentary successions surrounding the Dabie orogen to evaluate the exhumation history of the Dabie orogen. We use a state-of-the-art multi-proxy provenance analysis approach including sandstone petrography, heavy-mineral analysis, zircon and rutile U–Pb chronology and trace-element chemistry, as well as garnet and mica major-element chemistry. We show that the HP-UHP rocks contributed material to sediments in these basins peripheral to the Dabie orogen and integrate the results into a detailed palaeo-drainage framework.

2 | GEOMORPHIC-GEOLOGICAL SETTING AND STRATIGRAPHY

2.1 | Geomorphic and geological setting

The Qinling-Dabie-Sulu orogen is the natural climatic and geographical boundary between North and South China, and it represents the watershed between North and South China (Figure 1a). The Dabie orogen forms the easternmost part of the much larger Qinling-Dabie-Sulu orogen (Ratschbacher et al., 2003). The high topography of ~0.8–1.5 km in the Dabie orogen sharply decreases to the north and more gently to the south (Ding et al., 2021) to below 50 m in the hilly lowland NCC Plains and SCB, respectively (Figure 1b). The Dabie orogen is the watershed controlling the drainage pattern in eastern China with the Huai River receiving tributary drainage flowing northward from the Dabie orogen, and the Yangtze River receiving tributary drainage flowing southward and eastward from the Dabie orogen.

The Dabie orogen is one of the largest HP-UHP metamorphic terranes in the world, with an areal extent of >30,000 km^2 (Figure 1c; Li et al., 1993; Liou et al., 2009; Zhang et al., 2009; Zheng, 2008). Latest Permian metamorphic bedrock ages from the Dabie orogen have been extensively reported. These include a prograde 252 Ma titanite age (Gao et al., 2011) and ca. 255–263 Ma garnet Lu-Hf and muscovite $^{40}Ar/^{39}Ar$ ages (Cheng et al., 2011; Cheng & Vervoort, 2015; Liu et al., 2008). The timing of peak UHP metamorphism is constrained at 245–222 Ma (Kylander-Clark et al., 2012). The HP eclogite-facies recrystallisation and amphibolite-facies retrogression of the Dabie UHP rocks occurred at approximately 222–215 Ma and 215–205 Ma (Zheng, 2008), respectively. Rutile in coesite-bearing eclogites from the Dabie orogen range in age from 243 ± 5 Ma to 175 ± 6 Ma (1σ, 297 grains in total from the studies of Chen et al., 2022; Franz et al., 2001; Gao et al., 2014; Hou et al., 2016; Hou et al., 2020; Li, Li, Sun, & Zhang, 2003; Li, Li, Zheng, et al., 2003; Liu, Xiao, Wörner, et al., 2014; Shen, 2013; Xiong, 2016) and represent closure to Pb diffusion at ca. 500°C. Exhumation to below the $^{40}Ar/^{39}Ar$ closure temperature for white mica (ca. 300°C) continued until the earliest Middle Jurassic (ca. 178 Ma) in the Dabie orogen (Hacker & Wang, 1995). The Dabie orogen is separated from the SCB by the Xiangfan-Guangji fault and the strike-slip Tanlu fault zone to the southwest and east, respectively (Figure 1d). Motion on the Tanlu sinistral fault system initiated at 230–240 Ma and prolonged sinistral ductile shearing continued into the Early Cretaceous (Zhu et al., 2006), resulting in the present-day offset of more than 500 km between the Dabie orogen and the Sulu orogen. However, there remains a high degree of uncertainty on the amount of offset (see the review of Peng et al., 2022).

The Dabie orogen is composed of a series of fault-bounded terranes with different metamorphic *P–T* conditions. Zheng et al. (2005, 2019) divided the Dabie orogen into five main tectonic units (Figure 1d). These are from north to south: the Beihuaiyang terrane (a LT-LP greenschist–amphibolite-facies metamorphic belt, $T = 570$°C, $P = 0.71$ GPa), the north Dabie terrane (a HT-UHP eclogite-facies metamorphic belt, $T = 875$°C, $P = 4.50$ GPa), the central Dabie terrane (a MT-UHP eclogite facies metamorphic belt, $T = 613$–728°C, $P = 3.09$–3.87 GPa), the south Dabie terrane (a LT-(U) HP eclogite-facies metamorphic belt, $T = 600$–630°C, $P = 2.70$–2.90 GPa) (Xia et al., 2023) and the SuSong Complex (a LT-HP blueschist−greenschist-facies metamorphic belt, $T = 427$–532°C, $P = 0.34$–0.98 GPa) (Wu et al., 2023). All five zones are intruded by a voluminous suite of Early Cretaceous granitic plutons (Figure 1d; Jahn et al., 2003; Zheng et al., 2019), with minor occurrences of coeval volcanic rocks (Fan et al., 2004). The north Dabie terrane is the largest UHP litho-tectonic unit in the Dabie orogen. The UHP units of the central Dabie and north Dabie terranes have different crustal affinities, representing subducted upper and lower crust, respectively. The timing of prograde metamorphism, peak UHP metamorphism and retrograde metamorphism is in general younger to the north (Xu & Wang, 2019). The SuSong Complex was subducted to a depth of 20–40 km from 251 to 260 Ma and then

started to exhume, followed by the exhumation of the south Dabie terrane (236–242 Ma), the middle Dabie terrane (226–238 Ma) and the north Dabie terrane (170–226 Ma), representing continuous, oblique and differential exhumation (Shi et al., 2022).

The north Dabie, central Dabie and south Dabie terranes constitute the main body of the Dabie orogen, with widely exposed paragneiss, orthogneiss and migmatite. The HP and UHP meta-igneous rocks in the Dabie-Sulu orogen mainly yield Neoproterozoic protolith ages of 780–740 Ma with Triassic metamorphic ages, implying that the Neoproterozoic bimodal felsic–mafic igneous rocks of the SCB that formed during the breakup of the Rodinia supercontinent were subducted deep beneath the NCC, resulting in Triassic HP-UHP metamorphism (Zheng et al., 2019). Notably, no latest Palaeozoic–Early Mesozoic igneous and volcanic rocks occur either in the hanging wall (southern margin of the NCC) or within the Dabie-Sulu orogen (Wu & Zheng, 2013; Zheng et al., 2003, 2005).

The Dongling Complex is located to the southeast of the Dabie orogen (east of the Tanlu Fault, Figure 1d) and is the only metamorphic basement within the SCB in the Middle-Lower Yangtze Valley exposed at Earth's surface. The exposed area of approximately 30 km^2 (Chen & Xing, 2016) comprises quartz schists and granitic orthogneisses with a protolith age of ca. 1.85 Ga (Chen & Xing, 2016; Grimmer et al., 2003; Zhang et al., 2015).

2.2 | Stratigraphy of the basins

This study focuses on the Lower Jurassic of four sedimentary basins surrounding the Dabie orogen (Figure 2). These are the Hefei basin to the north of the Dabie orogen, the Nanjing basin to the northeast, the Yueshan basin to the east and the Huangshi basin to the south (Figure 1d). Except for the Hefei basin which is located on the basement of the NCC, the other three basins are located on the SCB in the Lower Yangtze region (Liu et al., 2003). The Lower Jurassic strata of the three basins located on the SCB were once part of a more widespread basin that was later segmented by faulting into its present configuration (Zhu et al., 2009). Geological maps showing the sampling locations are provided in Figure 2. The basin settings /

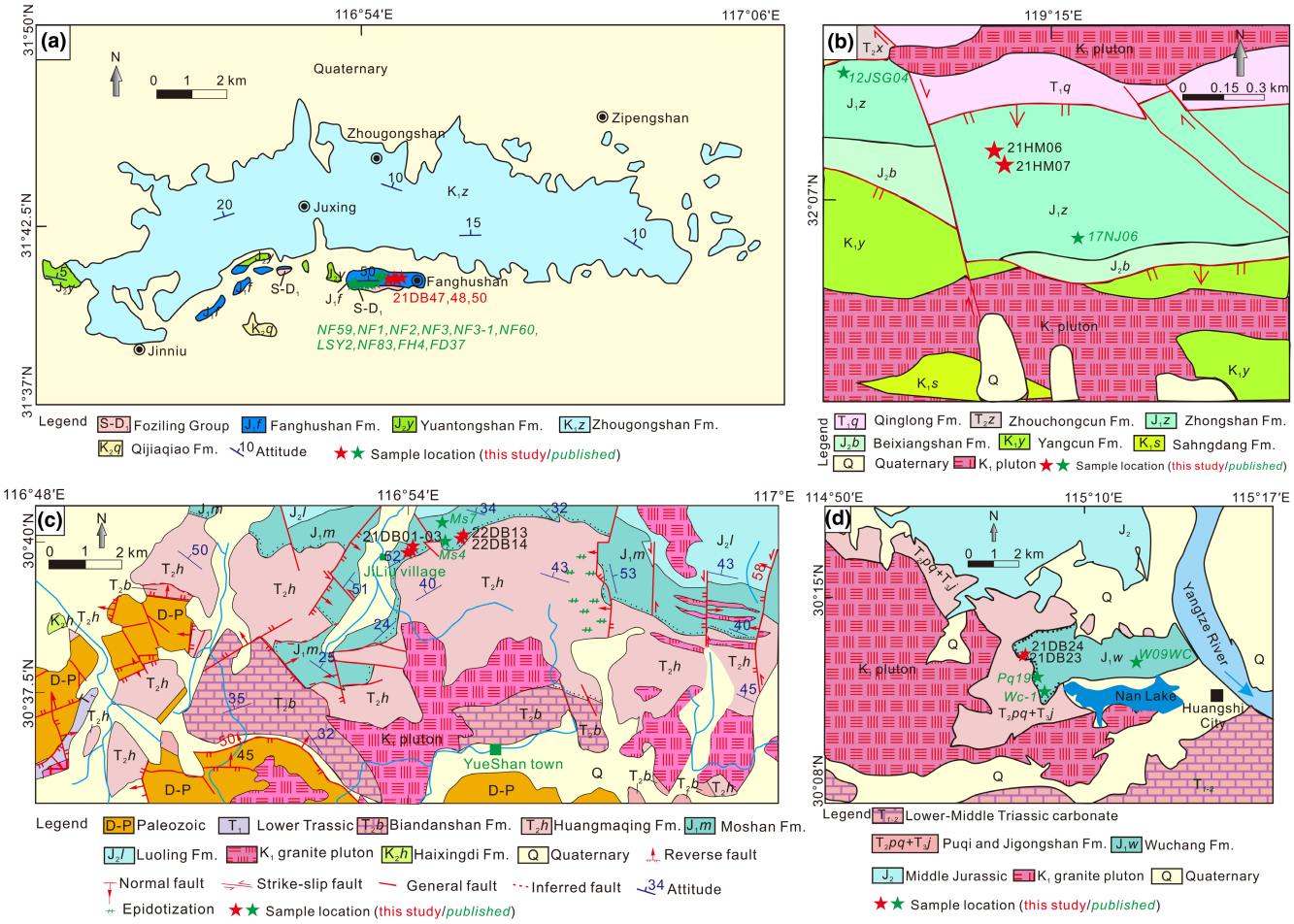

FIGURE 2 Detailed geologic maps of the sampled peripheral basins. (a) Hefei basin, (b) Nanjing basin, (c) Yueshan basin and (d) Huangshi basin. Sampling locations are indicated by red asterisks.

types and individual formations are briefly summarised below.

The Early Jurassic tectonic setting of the Hefei basin is controversial. Meng et al. (2007, 2019) suggest the Hefei basin was in an extensional setting that was triggered by upward extrusion of Dabie UHP to the south. Instead, many workers support a retro-foreland basin model (Liu et al., 2010). For the Nanjing, Yueshan and Huangshi basins, located on the foreland side of the Dabie orogen, a peripheral foreland basin model is widely accepted (Liu et al., 2003, 2005; Liu & Zhang, 2013). However the following key problems with a peripheral foreland basin model are noted: (1) There was no conclusive contemporaneous Early Jurassic fold-and-thrust belt controlling the formation of basins; (2) The Lower Jurassic sandstone composition lacks the contribution of unstable sedimentary lithics which are typical of foreland basins; (3) strata-thickness isopach maps (Figure 1d) do not show a typical asymmetric wedge-shape towards the orogenic belt. Therefore, considering the uncertainty on the tectonic setting of the basins, we use the generic term 'peripheral basins' in this study to emphasise that these sedimentary basins were distributed on the periphery of the Dabie orogen. This usage is widely adopted in other orogenic belts and their associated sedimentary basins (such as Calvet et al., 2021; Di Capua et al., 2021).

The oldest unit in the Hefei basin is the Fanghushan Formation (Li, Li, et al., 2004; Li, Zheng, et al., 2004), that contains plant and non-marine bivalves (Bureau of Geology and Mineral Resources of Anhui Province, Regional Geology of Anhui Province, People's Republic of China, Ministry of Geology and Mineral Resources, 1987) indicating an Early Jurassic age (Figure 3). It was deposited on the greenschist-facies Silurian-Devonian graphitic and quartz–mica schists of the Foziling Group. The Fanghushan Formation is about 500 m thick and formed in an alluvial fan and braided river environment (Liu et al., 2010; Liu & Zhang, 2013). The lower 30–40 m of the formation mainly consists of white and grey-yellow conglomerates. Metamorphic pebbles are generally

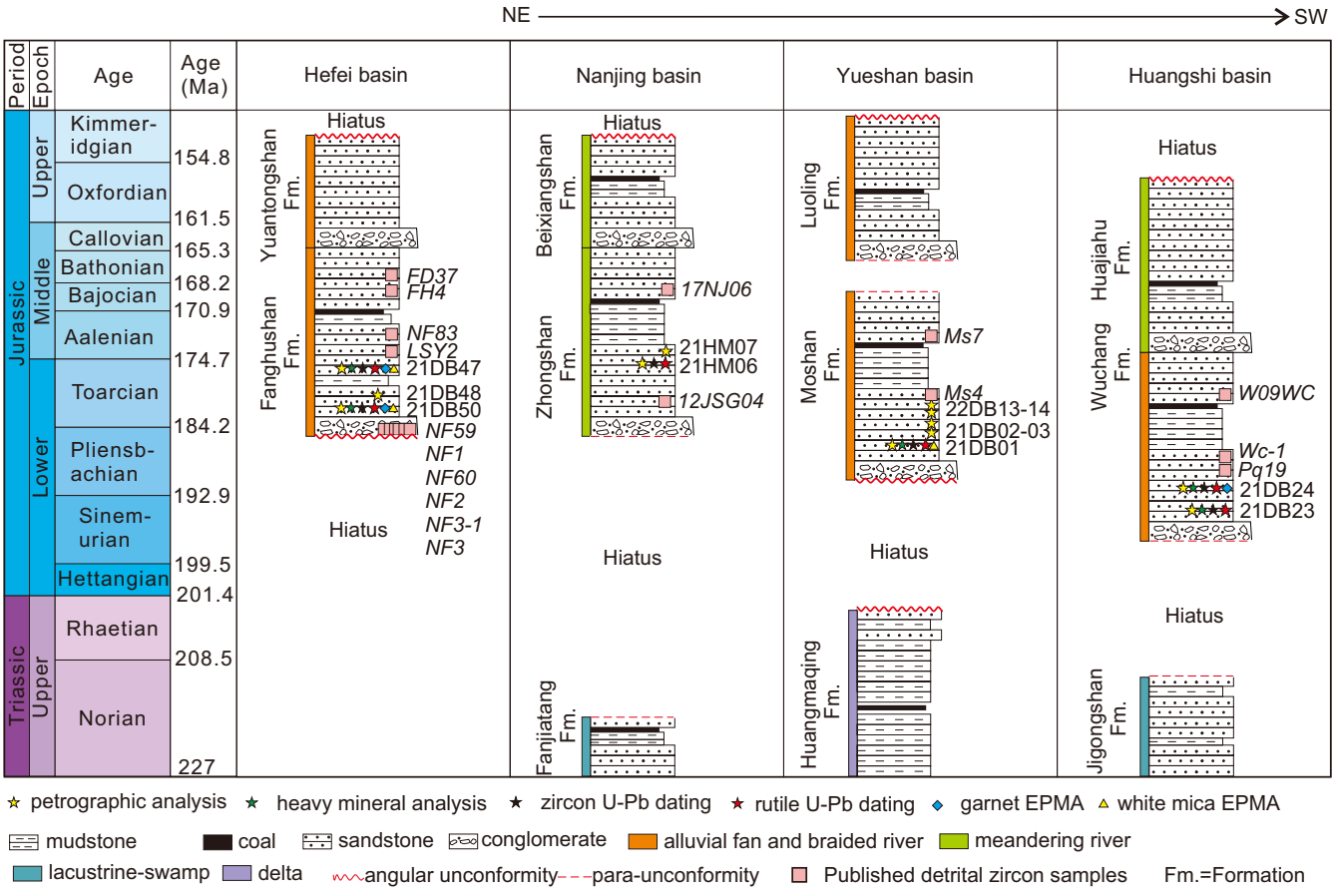

FIGURE 3 Generalised stratigraphic columns for the Lower Jurassic strata in the studied basins. Stratal ages follow the biostratigraphic–chronostratigraphic framework and correlation scheme established by Huang (2019), Huang et al. (2021). The sample positions for the detrital U–Pb, petrographic, heavy mineral, garnet and white mica EPMA analyses are shown schematically. Sample numbers compiled from other studies are listed, grouped by unit. Geological time scale adapted from the 2022/10 ICS International Chronostratigraphic Chart.

less than 20 cm in size and are imbricated. The conglomerate gradually passes upwards into pebbly sandstone, medium-coarse quartzo-feldspathic sandstone and argillaceous siltstone with carbonaceous mudstone and coal seams containing plant fossils and bivalves (Meng et al., 2007). Paleo-flow indicators are mainly to the north and northeast (Li et al., 2001; Meng et al., 2007). The Fanghushan Formation is conformably overlain by the Middle Jurassic Yuantongshan Formation which consists of conglomerates and purple-red coarse-grained sandstones.

In the Nanjing basin, the Jurassic strata include the Lower Jurassic Zhongshan Formation and the Middle Jurassic Beixiangshan Formation (Figure 3; Huang, 2000; Ju, 1987). A paraconformity separates the Zhongshan Formation from the underlying Late Triassic Fanjiatang Formation. The Zhongshan Formation consists of conglomerates, sandstones and mudstones with abundant plant fossils that were deposited in a meandering river system with clearly defined channels (Guo et al., 2014). The quartz conglomerate at the base of the formation is 1–3 m thick, with pebble sizes of 1–30 cm composed mainly of quartzite, quartz sandstone, siliciclastic fragments, black chert and small amounts of mudstone clasts (Guo et al., 2014). Based on plant fossils, Huang (2019) determined the lower parts of the Zhongshan Formation as mid-late Early Jurassic in age, and the upper parts as early Middle Jurassic.

The Yueshan basin strata include the Lower Jurassic Moshan Formation and the Middle Jurassic Luoling Formation (Figure 3). The thickness of the Moshan Formation varies greatly, from hundreds to thousands of meters, and is 650 m thick in our studied section. The succession consists of fluvial conglomerates, sandstones, lenticular coal seams and mudstones with abundant gymnosperms and bivalve fossils (Cao, 2000; Guo, 1984; Huang, 1983). The bivalve assemblage *Pseudocardinia-Ferganoconcha-Tutuella* shows features characteristic of the middle–late Early Jurassic to the early Middle Jurassic (Lu et al., 1985), or the Middle Jurassic (Wan, 1987). A total of 35 species have been identified in the Moshan flora, and there are 20 species in common with the Wuchang flora of the Huangshi basin (see below), with a similarity of 57.1% (Huang, 1988). Huang and Lu (1988) suggest that these two floras should be unified, and the differences between them are caused by east–west differentiation in the depression. The Middle Jurassic Luoling Formation unconformably overlies the Moshan Formation and is composed of purple-red and grey sandstone, calcareous siltstone and silty shale, with intercalated grey-white pebbly coarse sandstone and conglomerate at the base. It is rich in bivalves, gastropods and ostracod fossils (Cao, 2000).

The Jurassic Huangshi basin includes the Lower Jurassic Wuchang Formation and the Middle Jurassic Huajiahu Formation, which were deposited in a braided river environment with coal-seam deposits (Figure 3; Yang et al., 2009). The Wuchang Formation contains abundant bivalves and plant fossils (horsetails, true ferns, cycads, ginkgo biloba, conifers) indicating an Early Jurassic age (Hong, 1986; Huang & Lu, 1988; Wang, 1993; Zhang et al., 1982). The basal conglomerate of the Wuchang Formation contains pebbles (usually <15 cm) of quartzite and siliciclastic rocks, potentially indicating a relatively stable sedimentary environment with long-distance transport (Li, Li, Sun, & Zhang, 2003; Li, Li, Zheng, et al., 2003). The Wuchang Formation is in conformable contact with the overlying Middle Jurassic Huajiahu Formation (Yang et al., 2010).

In summary, although there are abundant fossils and a high-resolution biostratigraphic framework for these Jurassic continental basins, these terrestrial ecosystems nevertheless exhibit regional variations in facies and faunas which are more challenging to correlate than marine biozones. It is therefore difficult to accurately constrain the depositional age of such continental strata in the absence of interbedded volcanic ashes.

3 | SAMPLES AND METHODS

We undertook field logging in the four basins, including detailed descriptions and interpretation of sedimentary structures. More than 50 sandstones samples were collected for sandstone petrography, heavy-mineral analysis, zircon and rutile U–Pb geochronology and trace-element chemistry, and white mica and garnet major-element chemistry. Sampling locations are provided in Figure 2 and Table S1.

3.1 | Sandstone petrography

Twelve sandstones were selected for petrographic modal analysis. At least 400 detrital grains in each sandstone sample were point counted under a petrographic microscope following the Gazzi-Dickinson method (Ingersoll et al., 1984; Table S1). Point counts were separated into quartz, feldspar, rock fragments and matrix. Porosity, accessory minerals, authigenic minerals and cements were excluded. Medium to coarse gneissose and plutonic grains were counted to not lose potentially valuable source information, but these counts were not included in the summation to 100% for plotting provenance diagrams (Willan, 2003). Sandstone classification follows Garzanti (2019).

3.2 | Heavy-mineral analysis

Five sandstone samples (21DB47, 21DB50 from the Hefei basin, 21DB01 from the Yueshan Basin and 21DB23, 21DB24 from the Huangshi Basin) were selected for heavy-mineral (HM) analysis. Samples were sieved, and the 32–500 μm grain size fraction was used for HM analysis. The light and heavy minerals were separated by a centrifuge using Na-polytungstate (2.90 g/cm^3) and freezing with liquid nitrogen. The HM separates were mounted on a slide using Canada balsam and counted under an optical microscope at an appropriate regular spacing on each mount. At least 200 non-opaque detrital grains were counted in each sample to characterise the heavy-mineral assemblage (Garzanti & Andò, 2019), except for sample 21DB24 (177 grains). The GPS coordinates of sample localities, point counting results and heavy-mineral index values (Hubert, 1962; Morton & Hallsworth, 1994) are presented in Table S1.

3.3 | U–Pb dating and trace elements of detrital zircon

Mineral separation for detrital zircon and rutile analysis comprised standard techniques including jaw crushing, and separation using a water table, followed by a magnetic separator and heavy liquids. Zircons were hand-picked, mounted in epoxy, and ground and polished to half-thickness to expose grain interiors. We employed reflected and transmitted light petrography to identify grains for zircon U–Pb analysis.

Zircon U–Pb dating was conducted by LA-ICP-MS in the Hongchuang Exploration Technology Service Co., Ltd. (NHEXTS), Nanjing, China. Laser ablation employed a Resolution SE model (Applied Spectra, USA) equipped with an ATL (ATLEX 300) excimer laser and a two-volume S155 ablation cell. The laser ablation system was coupled to an Agilent 7900 quadrupole (Q)-ICP-MS (Agilent, USA). All analyses were conducted with a laser beam diameter of 30 μm, a 5 Hz pulse frequency, and a fluence of 2.5 J/cm^2. GJ-1 was used as the primary zircon age reference material (Jackson et al., 2004). In addition, a secondary age reference material 91,500 (^{206}Pb/^{238}U TIMS age of 1065.4 ± 0.6 Ma, Wiedenbeck et al., 1995) was analysed during every U–Pb run for quality control. During the course of analysis, the secondary reference material yielded a weighted average ^{206}Pb/^{238}U age of 1066.9 ± 7.5 Ma. Data reduction was carried out using the VizualAge (U–Th–Pb) (Petrus & Kamber, 2012) and Trace_Elements data reduction schemes (DRS), which operate within the IOLITE software package (Paton et al., 2011). Reported uncertainties are at the 2σ level. The reported ages are ^{206}Pb/^{238}U ages for grains younger than 1000 Ma and ^{207}Pb/^{206}Pb ages for grains with ages greater than 1000 Ma (cf Chew et al., 2020). Analyses with concordance <90% and >110%, and uncertainties >10% were excluded. U–Pb age kernel density estimate (KDE) spectra were produced using the software detritalPy (Sharman et al., 2018). U–Pb dating and trace-element analysis were undertaken on 835 zircon grains with 796 passing the concordance threshold. All analytical data, instrumental setup information and data on secondary reference zircons can be found in Table S1.

3.4 | U–Pb dating and trace elements of detrital rutile

Rutile was analysed by an Agilent 7900 Q-ICP-MS coupled to a Photon Machines Analyte Excite 193 nm ArF excimer laser-ablation system at Trinity College Dublin. Each grain was analysed for 25 s with a 10 s washout, which was employed for the baseline measurement. All data reduction was performed off-line using the IOLITE data reduction package with the VizualAge_UcomPbine (apatite and rutile) DRS (Chew et al., 2014). Full details of the data reduction methodology can be found in Paton et al. (2011) and Chew et al. (2014). For rutile U–Pb dating, R10 rutile (1091.6 ± 3.8 Ma for U–Pb TIMS age; Luvizotto et al., 2009) was employed as the primary age reference material, and R19 (^{206}Pb/^{238}Pb ID-TIMS age of 489.5 ± 0.9 Ma; Zack et al., 2011) and R13 (~510 Ma concordia age, Schmitt & Zack, 2012) were employed as secondary age reference materials and treated as unknowns during data reduction (Luvizotto et al., 2009). During the course of analysis, the secondary age reference materials yielded weighted average ^{207}Pb-corrected ages of 491.3 ± 6.6 Ma and 511.2 ± 4.3 Ma for R19 and R13 rutile, respectively. For detrital rutile unknowns, the Stacey and Kramers (1975) terrestrial Pb evolution model was used for the isotopic composition of initial Pb, and an iterative (^{207}Pb) common Pb correction was applied (Chew et al., 2011). Due to the ^{207}Pb correction, no rutile U–Pb age data can be excluded based on discordance criteria. However, the low-U contents (sometimes <1 ppm) and consequent near-zero radiogenic Pb content of some grains can result in large analytical uncertainties (or negative ages). For this reason, an empirical exclusion criterion as proposed by Chew et al. (2020) was applied, whereby only grains with a 2σ % uncertainty < "sample age" ×8× "sample age"$^{-0.65}$ were accepted for inclusion in the rutile KDE spectra. For rutile trace-element analysis, the Trace_Elements DRS was employed in IOLITE (Paton et al., 2011). The complete dataset is provided in Table S1. U–Pb dating and trace-element analysis were undertaken on 944 rutile grains, and due to low U and/or high common Pb contents, a total

of 521 rutile grains passed the age uncertainty threshold criterion.

3.5 | Electron probe micro-analyser

Two samples (21DB47, 21DB50) from the Hefei basin and one sample (21DB24) from the Huangshi basin were selected for detrital garnet analysis by electron probe micro-analyser (EMPA). Two samples (21DB47, 21DB50) from the Hefei basin and one sample (21DB01) from the Yueshan basin were selected for detrital white mica analysis by EMPA. Mineral compositions were analysed at the State Key Laboratory of Mineral Deposits Research, Nanjing University using a JEOL 8900 electron microprobe. The EPMA laboratory has a comprehensive set of oxide, carbonate, sulfide, sulfate, and native element reference materials that cover the majority of elements found in the periodic table. Measurements were performed with a 15 kV accelerating voltage, a 20 nA beam current, a 1 or 5 μm beam diameter, and a peak counting time of 60 s. Garnet and white mica cores and rims were analysed to test for intra-grain heterogeneity. Natural minerals were used as reference materials, and conventional ZAF correction procedures were applied. Relative errors for all elements are below ±1%. End-member compositions for white mica were calculated following Coggon and Holland (2002). Garnet end-member compositions were calculated following Locock (2008).

4 | RESULTS

4.1 | Sandstone petrology

Lower Jurassic sandstones from the Yueshan and Huangshi basins show low feldspar contents and predominantly are comprised of monocrystalline quartz, with minor polycrystalline quartz including diffuse and foliated varieties. The lithic composition between these two basins is very similar, and the lithics are almcsts and chert. Chert lithics contains abundant radiolarian fossils (Figure 4a–d). Metamorphic lithics show variable metamorphic grades ranging from cleaved quartz-muscovite schist (Figure 4e,f) to sericite-rich phyllitic fragments (Figure 4g). Some foliated, dynamically recrystallised quartzite lithics are present (Figure 4h,i). Seven sandstones plot in the litho-quartzose metamorphiclastic field with mean Q:F:L ratios of 83.6:0.2:16.2 (Figure 5a), and mean Lm:Lv:Ls ratios of 64.7:0.8:34.5 (Figure 5b).

In the Nanjing basin, the two sandstones (both from the Zhongshan Formation) are quartzose sandstones with mean Q:F:L ratios of 92.8:6.4:0.8. There are rare lithics (*L* are 0.0%–1.7%) of felsic volcanics and quartzite.

In the Hefei basin, the three sandstones (all from the Fanghushan Formation) are litho-quartzose metamorphiclastic sandstones with mean Q:F:L ratios of 76.3:3.7:20.0. Lithic grains generally comprise foliated and mica-rich metamorphic fragments (Figure 4j,m), dynamically recrystallised granite-gneiss fragments (Figure 4k–n) and sedimentary fragments including mudstones and sandstones (Figure 4o) with mean Lm:Ls:Lv ratios of 89.5:1.2:9.3 (Figure 4b). The rare granitic gneiss fragments show a granoblastic texture with gneissic structure. The main mineral grains are potassium feldspar, elongated and deformed undulose quartz, and muscovite. Cracks are commonly developed on the surfaces of monocrystalline quartz (Figure 4o).

4.2 | Heavy-mineral assemblages

All five samples show a high amount of ultra-stable heavy-minerals with a ZTR index (zircon + tourmaline + rutile) ranging from 87% to 100%, with an average of 97% (Table S1). Except for one sample from the Yueshan basin (21DB01) that shows a very high dravite content (84%), all other samples show strong enrichment in zircon (58.9%–94.2%, Figure 5c). All five samples have some amount of rutile in varying proportions (0.9%–16.7% of the total transparent heavy minerals). Garnet is present but very rare (no garnet grains in the counted 200 non-opaque heavy-mineral grains). This is in agreement with Li et al. (2000), who detected only three garnet grains in a large sample of grains from a Fanghushan Formation sandstone.

4.3 | Detrital U–Pb zircon and rutile geochronology

In the Hefei basin, sample 21DB50 from the lowermost Fanghushan Formation displays prominent zircon U–Pb age peaks at ca. 449 Ma, 753 Ma and 1.95 Ga, with one solitary Triassic (250 Ma) grain (Figure 6). The rutile U–Pb ages show a minor Triassic age peak at ca. 244 Ma (seven grains), a major population at ca. 450–490 Ma with the remainder of grain ages ranging from 179 Ma to 1943 Ma. Sample 21DB47 from the upper Fanghushan Formation show two main zircon U–Pb populations in the Triassic (230 Ma, 28% of all grains) and in the Neoproterozoic (776 Ma). In the rutile U–Pb age population, although comprised by only 26 grains in total, 20 grains (77%) define a Triassic peak at 214 Ma, with five rutile grains (19% of all grains) yielding Jurassic ages spanning 167–195 Ma.

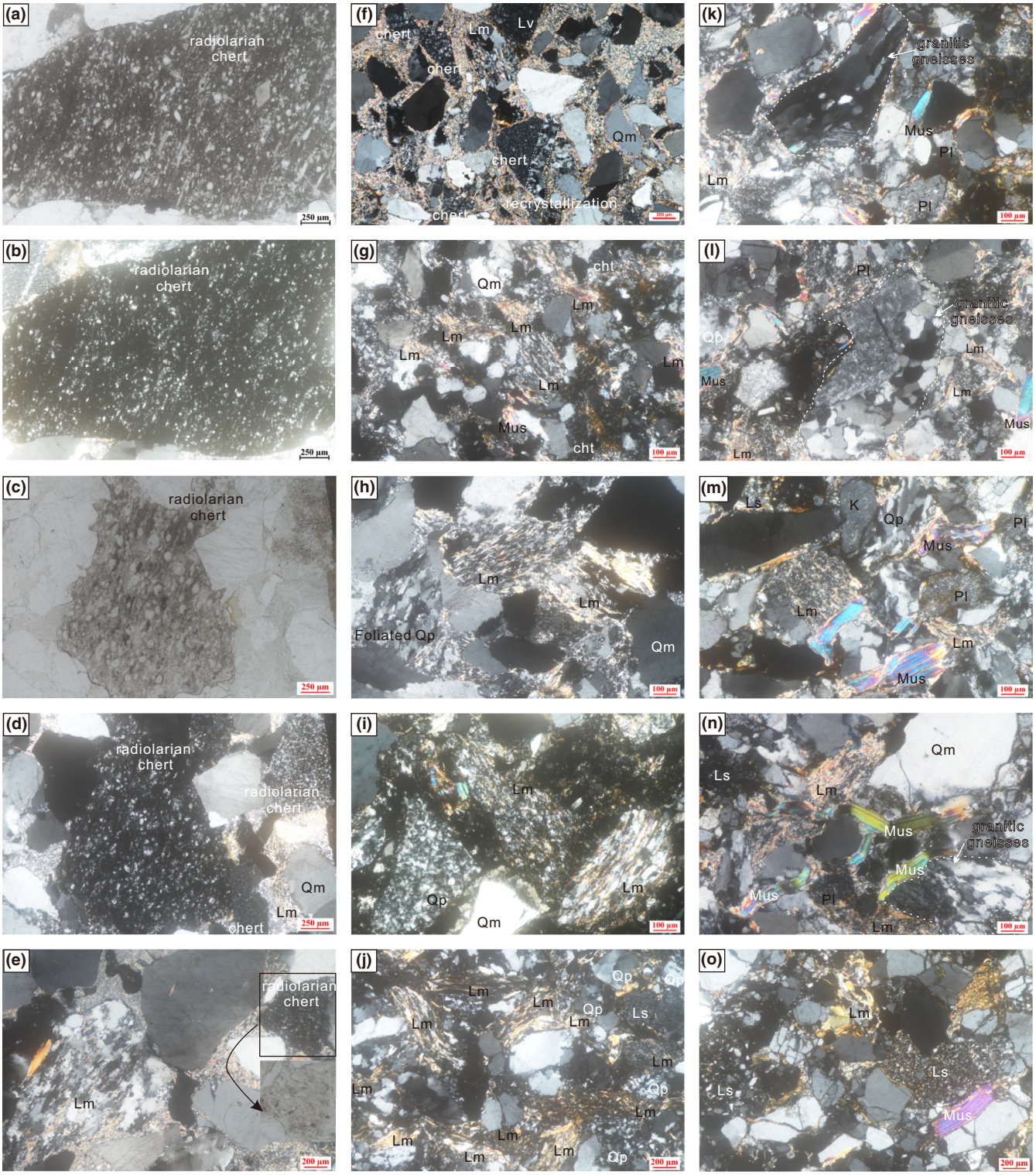

FIGURE 4 Petrographic photomicrographs. (a–d) Chert fragments in litho-quartzose sandstone (21DB01 and 21DB02, respectively), the corresponding plane-polarised and cross-polarised photographs are shown. (e–i) Litho-quartzose sandstone from the Yueshan and Huansghi basins (21DB03, 21DB23, 21DB24, 22DB13, and 22DB14, respectively); (j–o) Litho-quartzose sandstone from the Hefei basin (21DB48, 21DB47, 21DB50, 22DB48, 22DB50 and 22DB47, respectively). Qm = monocrystalline quartz, Qp = polycrystalline quartz, Pl = plagioclase, K = K-feldspar, Mus = muscovite, Cht = chert, Ls = terrigenous clastic fragments, Lm = metamorphic fragments.

In the Nanjing basin, the detrital zircon spectra from the Lower Jurassic sample (21HM06) from the Zhongshan Formation are dominated by Precambrian grains (>539 Ma, 77% of the total) grains, particularly Paleoproterozoic grains. There are two subordinate Phanerozoic peaks at 252 Ma and 424 Ma. The detrital rutile U–Pb spectra from

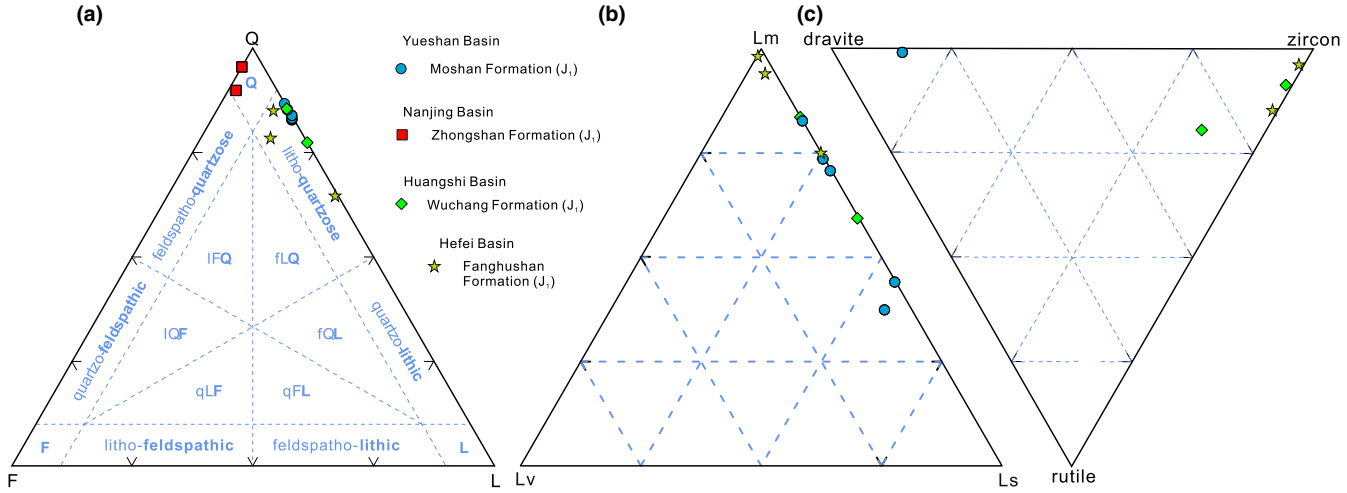

FIGURE 5 Petrography and heavy-mineral composition. (a,b) Petrographic ternary diagrams for the Lower Jurassic sandstones. Q = quartz, F = feldspar, L = lithic fragments (Lm = metamorphic, Ls = sedimentary, Lv = volcanic). (c) Ternary plot for the heavy-mineral assemblages.

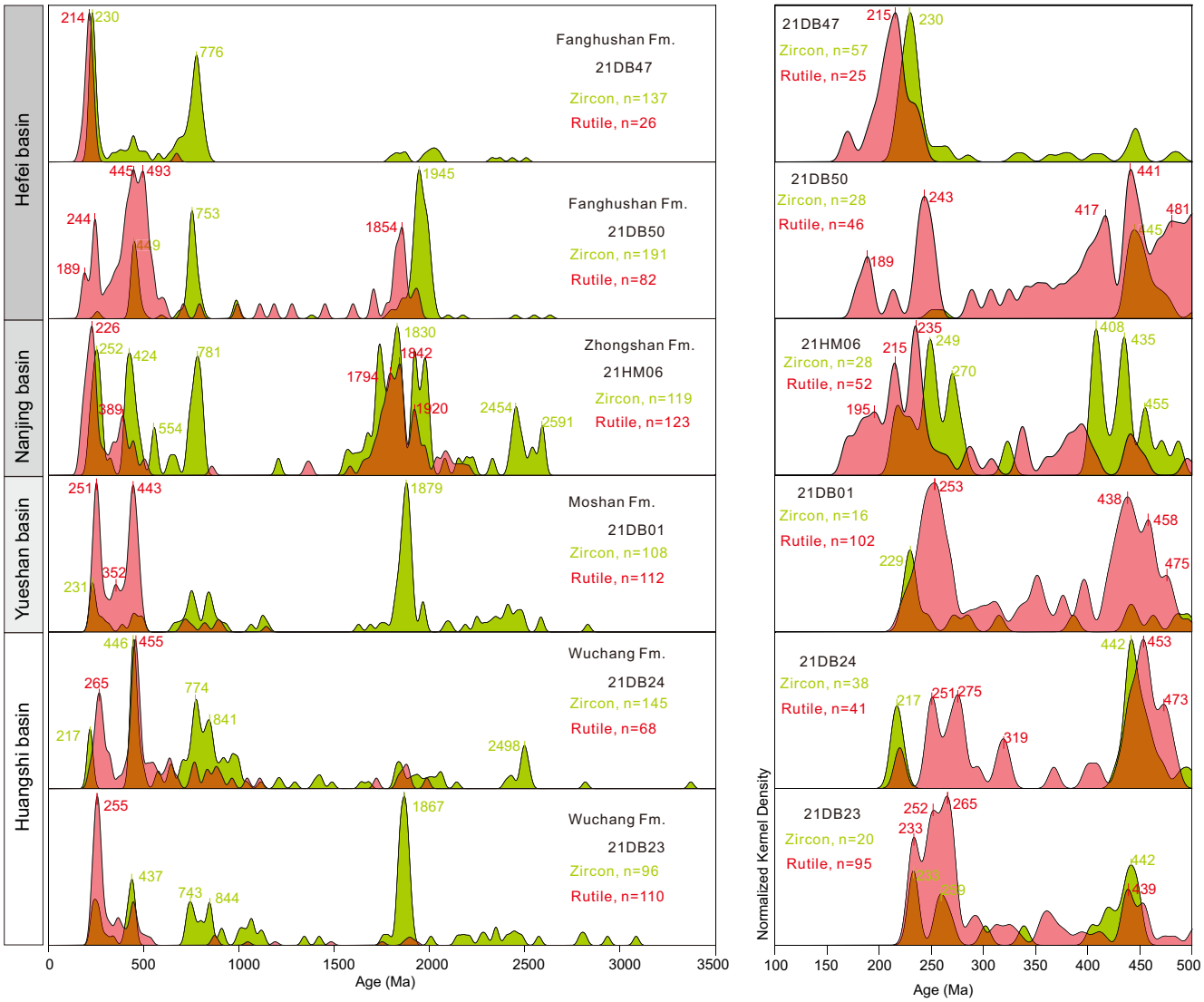

FIGURE 6 Normalised Kernel density estimate (KDE) diagrams for the detrital U–Pb age distributions. Samples are stacked in stratigraphic order for each basin. All ages are displayed in the left column with a 15 Ma bandwidth, and ages from 100 to 500 Ma are additionally shown with a 5 Ma bandwidth on the right column.

the same sample yield two prominent U–Pb age populations centered at 226 Ma and ca. 1.7–1.9 Ga, with a minor population at 389 Ma (Figure 6).

In the Yueshan basin (sample 21DB01), the zircon U–Pb spectra are dominated by Paleoproterozoic grains with a major peak at 1879 Ma, along with two subordinate peaks at 231 Ma and 751–840 Ma (Figure 6). The detrital rutile U–Pb ages from the same sample show two significant Permo-Triassic (201–299 Ma, centered at 251 Ma, 34% of the total) and older (ca. 400–500 Ma, centered at 443 Ma, 38% of the total) age components, along with a subordinate peak at 352 Ma.

In the Huangshi basin, the Early Jurassic sample (21DB23) from the lowermost Wuchang Formation exhibits a multimodal zircon age spectrum with a Paleoproterozoic (1.6–2.5 Ga, 46% in the total) age population centered at 1867 Ma. Early Palaeozoic (437 Ma) and Neoproterozoic (743–844 Ma) ages are subordinate. Minor Triassic (four grains, 4% of the total, peak at 233 Ma) and Permian (four grains, 4% of the total, peak at 259 Ma) zircon age peaks are also present (Figure 6). The rutile U–Pb age spectra of the same sample show a latest Permian peak at 255 Ma (56% of the total) in a Kernel Density Estimate (KDE) with a 15-Myr bandwidth, but multiple peaks in the Permo-Triassic (233, 252, 265 Ma) for a 5-Myr KDE bandwidth. The stratigraphically higher sample (21DB24) from the Wuchang Formation exhibits Triassic (peak at 217 Ma, 6% of the total), Palaeozoic (peak at 446 Ma) and Neoproterozoic (peak at ca. 774–841 Ma) zircon age populations with minor and dispersed Paleoproterozoic ages. The rutile U–Pb age spectrum also has two significant populations in the middle Permian (265 Ma) and Early Palaeozoic (455 Ma). Five Triassic rutile grains (218–251 Ma, 7% of the total) are also recognised in sample 21DB24.

4.4 | Rutile trace elements

The Cr/Nb ratio of rutile is widely used as a provenance tracer, being higher in rutile from mafic rocks and lower in rutile derived from metapelites (Pereira & Storey, 2023; Tomkins et al., 2007; Triebold et al., 2012). Following Triebold et al. (2012), the equation $X = 5 \times (\text{Nb [ppm]-500)-Cr [ppm]}$ discriminates rutile source lithologies (where $X > 0$ for metapelites (e.g. low-medium grade metasediments, felsic granulites and paragneisses) and $X < 0$ for metabasites [e.g. eclogites and mafic granulites]). The rutile in the six detrital samples is predicted to be dominantly (59%–91%) sourced from metapelitic rocks but there are large differences between the basins (Figure 7a). Rutile from the Hefei and Nanjing basins shows a comparatively high proportion of metamafic source rocks (355%–42% and 30%, respectively), while only 13%–16% of the rutile in the Huangshi basin is derived from metamafic rocks. In the Yueshan basin, only 9% of the rutiles are assigned to a metamafic source. With regard to the U–Pb ages (filtered based on age uncertainties), Jurassic rutile comprises the highest proportion of metamafic sources (67%), followed by Triassic rutile (31%, Figure 7b). The majority of the Pre-Triassic rutile is assigned to a metapelitic source and there is no apparent correlation observed between age and Cr and Nb concentrations (Figure 7b). The Zr-in-rutile (ZIR) geothermometer can constrain the crystallisation temperature of rutile grains, and thus yield constraints on the metamorphic conditions in potential source area(s) (Zack et al., 2011). We used the combined dataset calibration of Kohn (2020) and an assumed pressure of 1.3 GPa. Although pressure has a significant effect on the ZIR thermometer (Kohn, 2020; Tomkins et al., 2007; Zack & Kooijman, 2017), in detrital rutile studies the host rock information including potential independent pressure constraints has been lost. We therefore employ a default pressure of 1.3 ± 0.5 GPa following Pereira and Storey (2023), which results in a divergence of less than 65°C (maximum value) from the calibration for β-quartz and coesite at a pressure $P = 3$ GPa (Kohn, 2020; Table S1).

ZIR temperatures show distinct sub-clusters among some age groups (Figure 7c). Rutile grains between 1.7 and 2.0 Ga exhibit high temperatures of >750°C. From ca. 470 Ma to ca. 270 Ma, average ZIR temperatures show a minor decline from 700 to 640°C. For rutile ages between ca. 270 and 230 Ma, ZIR temperatures define two populations at 450–570°C and 630–770°C. For rutile grains younger than ca. 215 Ma, the ZIR temperatures are all lower than 600°C, clustering at 530–550°C (Figure 7c). There is no clear correlation between source rock protolith (i.e. mafic vs. pelitic) and ZIR temperatures (Figure 7d).

4.5 | Zircon trace element results

The presence of metamorphic zircons in sediments is essential to trace the exhumation of UHP metamorphic rocks in orogens. Zircon CL images, Th/U ratios and chondrite-normalised REE patterns are effective methods for detecting such metamorphic zircons. Most magmatic zircons are characterised by a Th/U ratio of >0.4, although, there are many exceptions to this threshold (Hoskin & Schaltegger, 2003; Kirkland et al., 2015). By contrast, most metamorphic zircons are characterised by a Th/U ratio of <0.1 (Rubatto, 2017; Wu & Zheng, 2004).

In the Hefei basin, Triassic (215–250 Ma) zircon grains have very low Th contents (4.4–41.8 ppm), Th/U

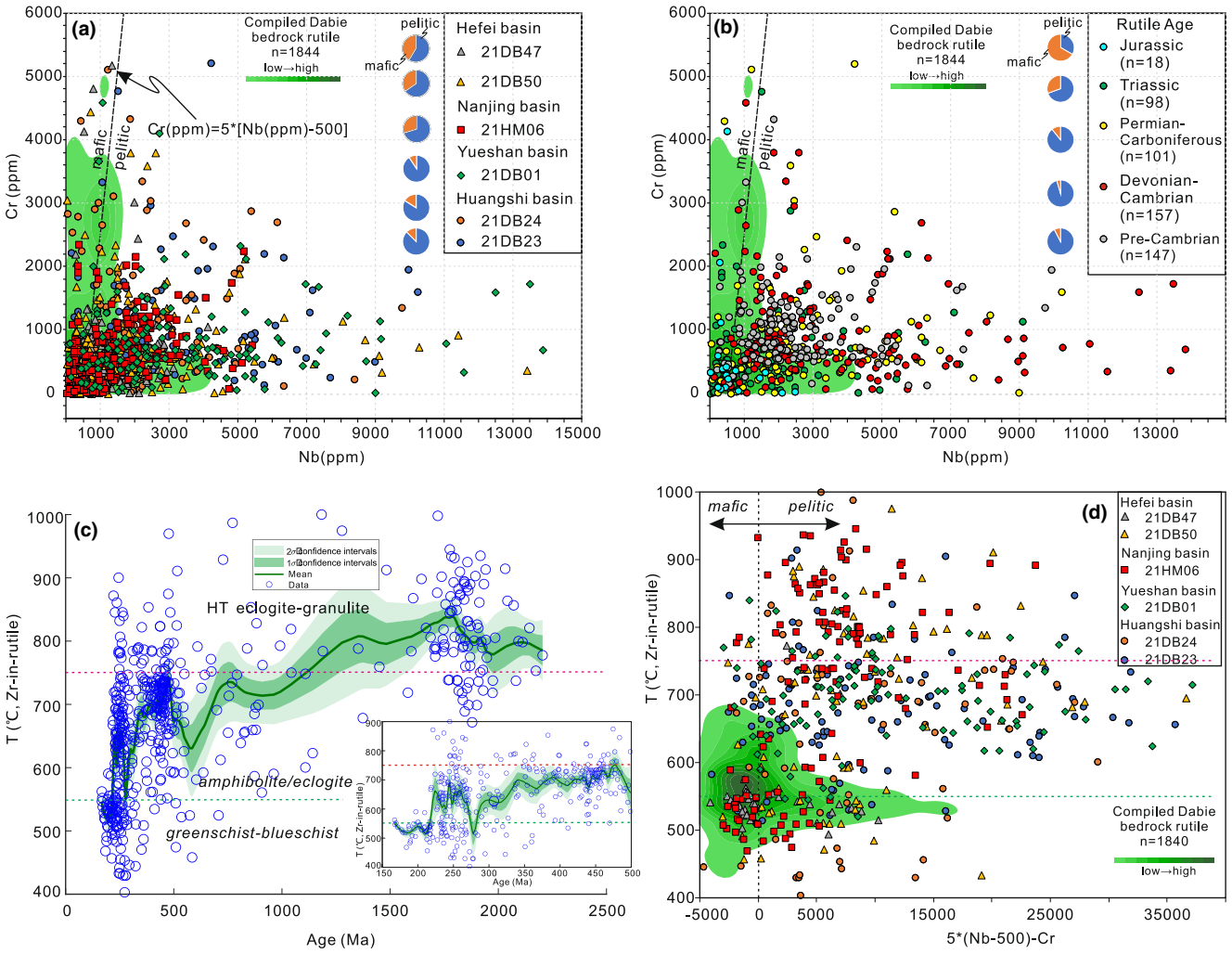

FIGURE 7 Trace-element analysis of detrital rutile from the Lower Jurassic strata. (a) Cr versus Nb discrimination plot of rutile protoliths after Triebold et al. (2012) using all detrital rutile trace- element analyses. Pie charts illustrate the proportions of pelitic versus mafic rutile. For comparison, a compiled Dabie bedrock rutile dataset is also shown. (b) Same plot using only filtered concordant rutile analyses with colour-coded ages. (c) Zr-in-rutile (ZIR) temperatures using the geothermometer of Kohn (2020) calculated at 1.3 GPa, plotted against U–Pb ages of detrital rutile analyses which pass the age uncertainty threshold. ZIR trends fitted by bootstrapping with 203.7 Ma windows for the 0–2500 Ma age range, and 33.2 Ma windows for the 150–500 Ma range (inset). 1σ and 2σ confidence intervals are shown as green bars. The bootstrapped moving ZIR averages were generated using the Acycle software (Li et al., 2019) with 10% loess regression. (d) ZIR temperatures plotted against protolith discrimination based on Cr and Nb trace-elements for rutile analyses which pass the age uncertainty threshold, positive 5×(Nb [ppm]-500)-Cr [ppm] values suggest sourcing from metapelitic rocks, while negative values suggest sourcing from metamafic rocks (Triebold et al., 2012). Note the compiled Dabie bedrock rutile geochemistry used for comparison with calculated temperatures within the α-quartz stability field at 1.3 GPa (Kohn, 2020). The trace element data of bedrock rutile in Dabie orogen are from Chen et al. (2022); Chen and Li (2008); Gao et al. (2010); Gao et al. (2014); Guo et al. (2012, 2017); Hou et al. (2022); Huang et al. (2012); Liang et al. (2009); Liu, Xiao, Aulbach, et al. (2014); Liu, Xiao, Wörner, et al. (2014); Sassi et al. (2000); Schmidt et al. (2009); Xiao et al. (2006); Yu, Chen, et al. (2006); Yu, Xu, et al. (2006); Zhang et al. (2008); Zheng et al. (2011); Zhu, Liang, et al. (2017) (see Table S1).

ratios (0.01–0.12) and total REE contents (19–190 ppm) (Figure 8a), as commonly observed in metamorphic zircon domains (Rubatto, 2017). These metamorphic zircons have flat heavy rare earth element (HREE) patterns (chondrite-normalised Yb_N/Gd_N ratios of 3.31–32.0) and mostly absent Eu anomalies ($Eu/Eu^*=0.51–0.76$, where $Eu/Eu^*=2\times Eu_N/(Sm_N+Gd_N)$), reflecting growth in the presence of garnet and absence of plagioclase, that is eclogite-facies metamorphism (Rubatto, 2017). Some ca. 1.8 Ga grains in sample 21DB50 are characteristic of high temperature granulite-facies zircon with slightly elevated flat HREE patterns (Figure 8b).

For the Nanjing basin, only two Triassic grains with low Th contents (3.8–14.8 ppm) and Th/U ratios (0.02–0.03) are observed (Figure 8c). They have shallow positive slopes from the MREE to HREE ($Yb_N/Gd_N=7.0–10.9$)

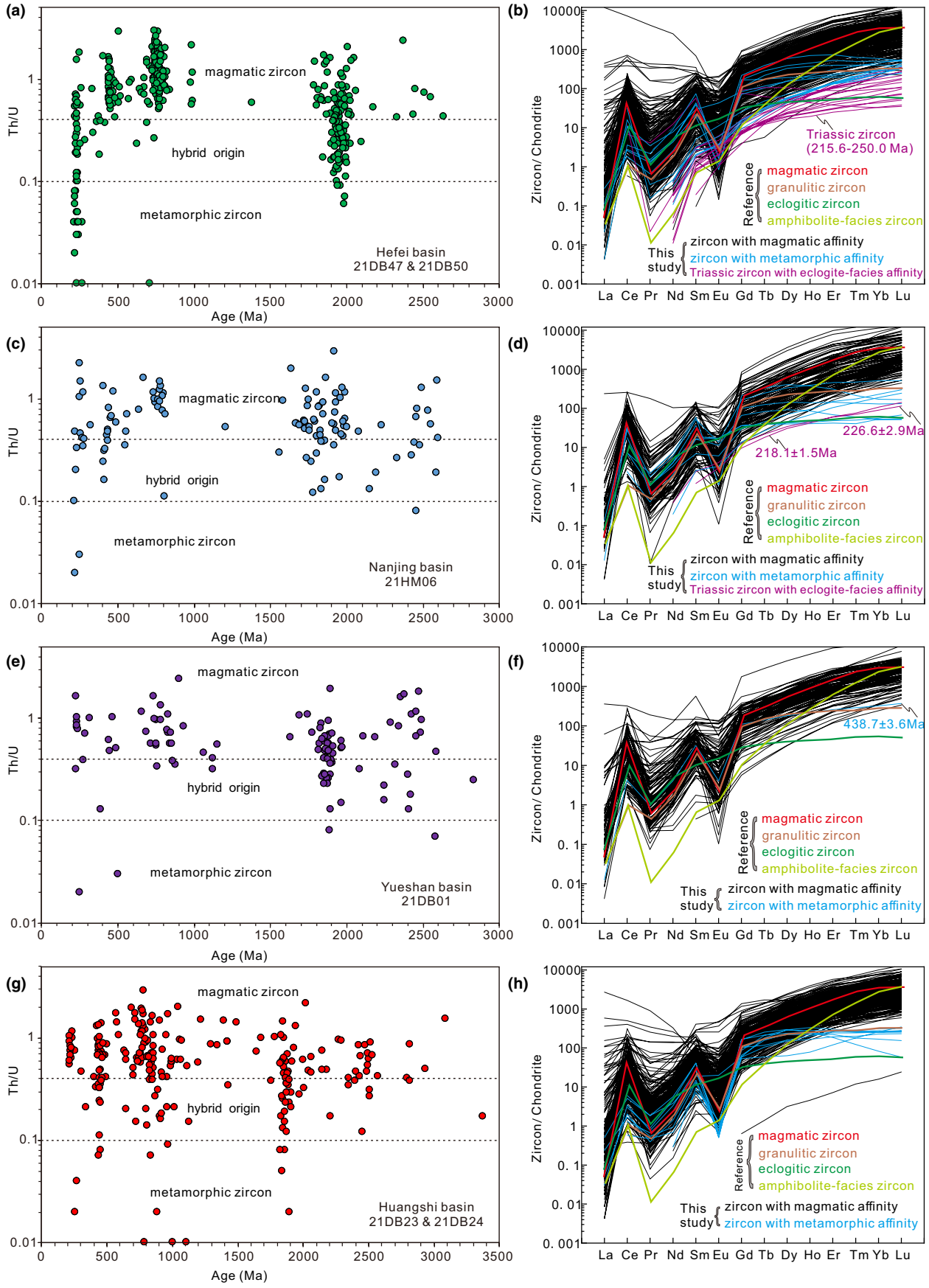

FIGURE 8 Zircon trace-element composition. (a, c, e, g) Zircon Th/U ratio versus age. (b, d, f, h) Chondrite-normalised rare-earth-element patterns. Chondrite data are from Sun and McDonough (1989). The REE patterns are plotted for the eclogite-, granulite- and amphibolite-facies to illustrate the competition for REE and its impact on the metamorphic zircon REE signature (Rubatto, 2017).

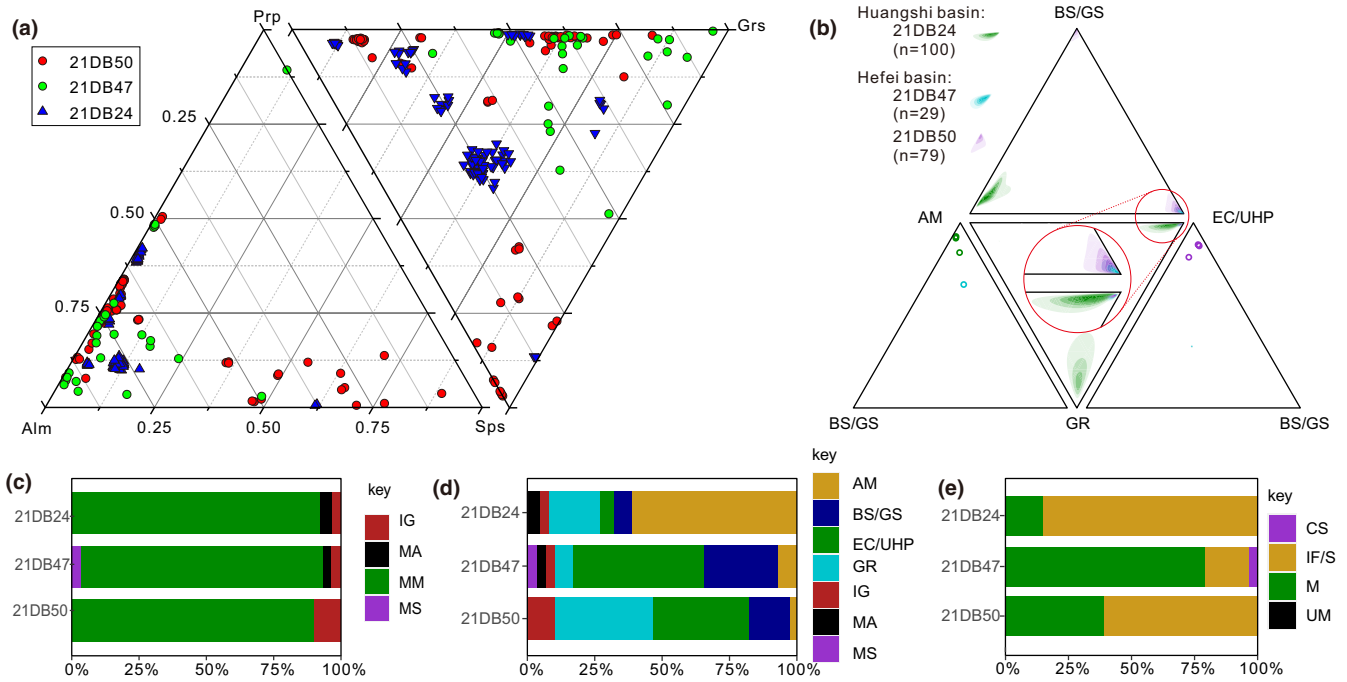

FIGURE 9 Detrital garnet major-element composition and discrimination. (a) Ternary diagrams considering the main endmembers almandine (Alm), spessartine (Sps), grossular (Grs), and pyrope (Prp). (b–e) Detrital garnet discrimination using the machine-learning model of Schönig et al. (2021). (b) Votes for specific 'metamorphic facies' classes, for garnets classified as MM (metamorphic) in (c), shown as kernel density estimate maps in four ternary diagrams that represent the sides of a tetrahedron. Point markers of individual datapoints are used for those ternary diagrams that include ≤5% of the data from the individual samples. (c) Proportions of garnet assigned to an igneous (IG), mantle (MA), metamorphic (MM), and metasomatic (MS) sources, based on the maximum votes. (d) Proportions of garnets assigned to amphibolite-facies (AM), blueschist–greenschist-facies (BS/GS), eclogite–ultrahigh-pressure-facies (EC/UHP), and granulite-facies (GR) metamorphic sources (see votes in [b]). (e) Proportions of the garnet 'composition' model assigned to calc–silicates (CS), intermediate–felsic/metasedimentary (IF/S), ultramafic (UM), and mafic (M) sources.

without significant Eu anomalies (Eu/Eu* = 0.55–0.56) when compared to magmatic zircon crystals (Figure 8d). No diagnostic Triassic metamorphic zircons have been recorded in the Yueshan and Huangshi basins (Figure 8e,g), although metamorphic zircons dated at ca. 440 Ma are present (Figure 8f,h).

4.6 | Garnet and white mica EPMA results

Most garnets show a compositionally homogeneous cross-sectional profile without zoning, with almandine as the dominant endmember (0%–86%, median is 62%) followed by pyrope (0.5%–42%, median is 14%), grossular (0%–96%, median is 8%) and spessartine (0.4%–89%, median is 3% (Figure 9a; Table S1). Following the discrimination scheme of Schönig et al. (2021), most garnet grains from the three samples originate from metamorphic rocks (90%–92%) (Figure 9c). For the Hefei basin, the detrital garnets show the highest probability of belonging to the eclogite/UHP-facies (48% and 35% for sample 21DB47 and 21DB50, respectively) and the granulite-facies groups (7% and 37%), while 28% and 15% respectively are assigned to the blueschist/greenschist-facies group (Figure 9b,d). In contrast, most garnet grains from the Huangshi basin (sample 21DB24) are assigned to the amphibolite-facies group (61%), followed by the granulite-facies group (19%), and only 5% of the garnets are assigned to the eclogite/UHP-facies group. Based on the garnet composition model classification sample 21DB47 has the most mafic garnet (79%), sample 21DB50 has 39% and sample 21DB24 has the least mafic garnet (15%) (Figure 9e).

Detrital muscovite ($n = 233$) is characterised by SiO_2 ranging between 43.9 and 54.8 wt.%, corresponding to 3.1–3.6 Si atoms per formula unit (pfu), with Al ranging from 1.9 to 2.9 pfu. Linear correlation graphs of Al versus Si indicate two compositional groups, one showing Si contents of 3.0–3.2 pfu and Al contents of 2.3–2.9 pfu, and the other showing higher Si (3.3–3.6 pfu) but lower Al (1.8–2.3 pfu) (Figure 10a–c). While both groups are present in the Yueshan and Huangshi basins (Figure 10a,c), the lower Si group is only a minor component in the Hefei basin (Figure 10b).

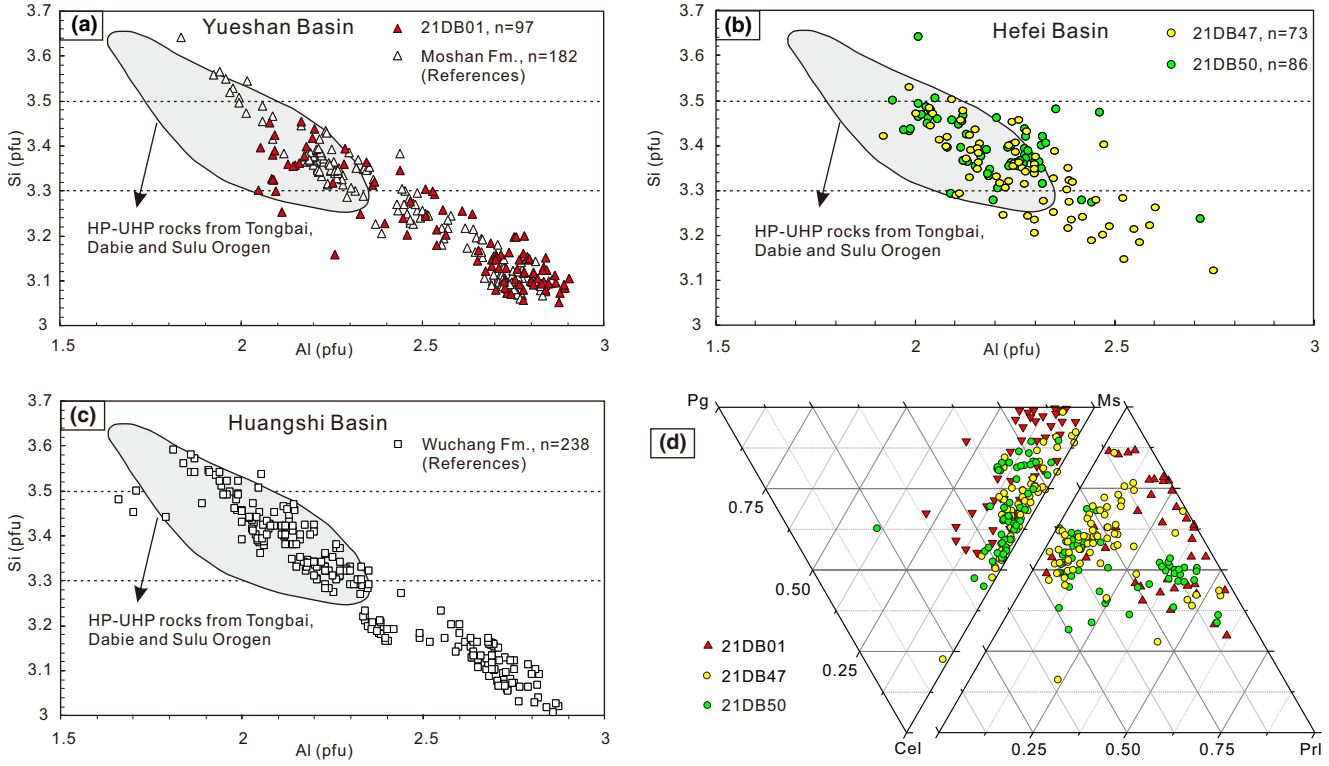

FIGURE 10 Detrital white mica composition. (a–c) Si versus Al diagrams for individual basins. Published detrital white mica data from Grimmer et al. (2003) and Zhu et al. (2006) for the Yueshan and Huangshi basins. Bedrock white mica fields after Wang et al. (2009). (d) Ternary composition diagrams for detrital white mica, muscovite (Ms)—paragonite (Pg)—celadonite (Cel)-Pyrophyllite (Prl).

The Tschermak substitution $[2Al^{3+} = Si^{4+} + (Fe, Mg)^{2+}]$ between muscovite and celadonite and the pyrophyllitic substitution $[Al^{3+} + K^{+} = Si^{4+}]$ accounts for most of the compositional variation (Figure 10d). Calculated mole fraction portions of the end-members are muscovite $X_{Ms} = 0.10–0.87$, celadonite $X_{Cel} = 0.02–0.52$, pyrophyllite $X_{Prl} = 0.00–0.56$, paragonite $X_{Pg} = 0.05–0.41$ (Table S1). The chemical composition of K-white mica is centered along the muscovite-celadonite join in the Ms-Pg-Cel triplot. Although there are significant differences between the three samples, there are no systematic trends when comparing each end-member for any of the individual samples (Figure 10d).

5 | DISCUSSION

5.1 | Provenance analysis of the Lower Jurassic sandstones

Detrital zircon U–Pb ages (7941 grains) from pre-Jurassic sedimentary and metasedimentary units from, or adjacent to the Dabie orogen are summarised here to evaluate their relationship to the Lower Jurassic strata as potential correlatives or source units (Figure 11). Detrital mineral U–Pb or Ar/Ar age data are grouped in one composite KDE for each basin in Figure 11, and also incorporate previously published detrital zircon U–Pb and phengite Ar/Ar ages (1339 zircon grains and 112 phengite grains) from Lower Jurassic units (Grimmer et al., 2003; Li et al., 2005; Li & Hu, 2022; She et al., 2012; Wang et al., 2009, 2020; Yang et al., 2010; Zhang et al., 2017; Zhu, Wang, et al., 2017) to evaluate their similarity and the relative contribution of each source area to the Lower Jurassic basins.

5.1.1 | Hefei and Nanjing basins

For the Hefei Basin, a large number of provenance studies have shown that the Lower Jurassic Fanghushan Formation contains Triassic coesite-bearing zircon (Chen et al., 2005; Li et al., 2005), indicating a provenance contribution from HP-UHP metamorphic rocks in the Dabie orogen. This is supported by our data, as shown by the presence of abundant Triassic eclogite-facies zircon (Figure 8a,b), Jurassic–Triassic rutile (Figure 6) with metamafic affinities (Figure 7a,b), eclogite-facies garnet (Figure 9b,d) of mafic affinity (Figure 9), high-Si phengite (Figure 10b,d) and foliated micaceous metamorphic fragments and

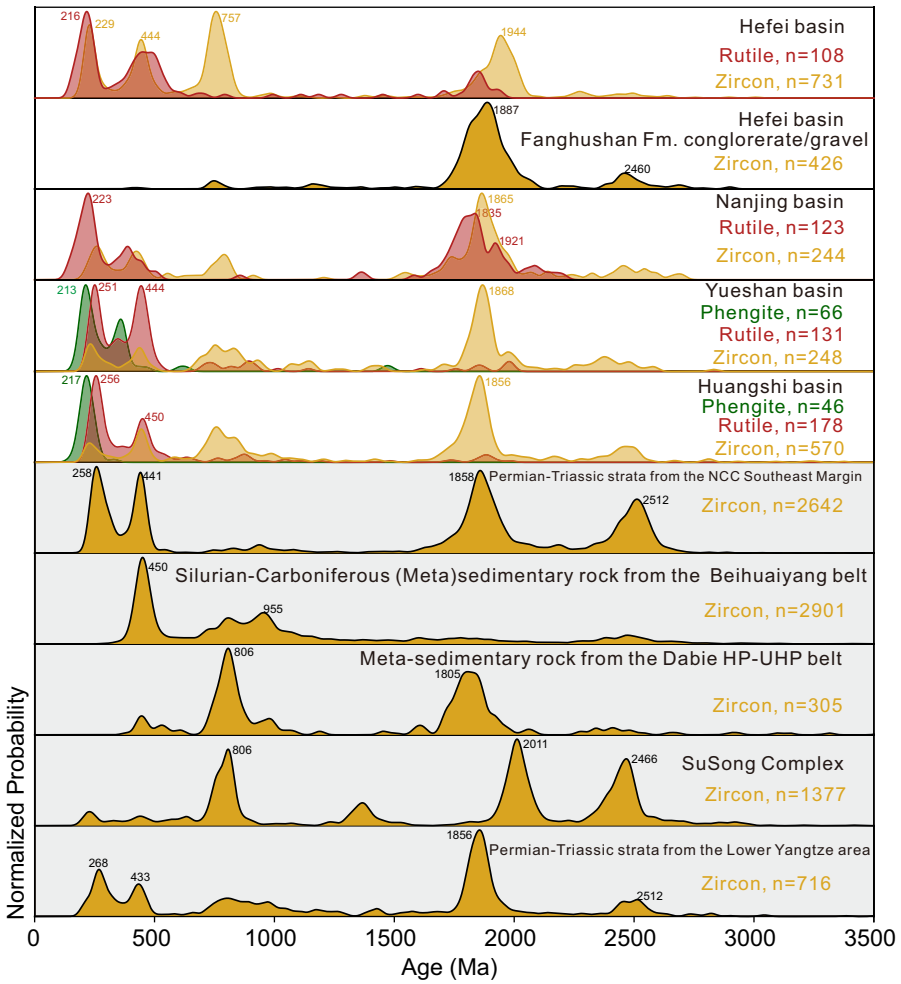

FIGURE 11 U–Pb and Ar—Ar age compilation. Data from the Lower Jurassic strata surrounding the Dabie orogen are compared with Palaeozoic-Mesozoic strata from the southeast margin of the NCC, Beihuaiyang belt, Dabie HP-UHP belt, SuSong Complex and Lower Yangtze area, both from this study ($n = 1413$) and the literature ($n = 9021$). Data shown as normalised KDE plots (fixed 20 Ma bandwidth) with labelled modal age peaks. Published data sources for the Lower Jurassic basins peripheral to the Dabie orogen are: Grimmer et al. (2003); Li and Hu (2022); Li et al. (2005); She et al. (2012); Wang et al. (2009); Wang et al. (2020); Yang et al. (2010); Zhang et al. (2017); Zhu, Wang, et al. (2017). Data sources for potential source regions comprise 46 references listed in Table S1.

granitic gneiss fragments in the sandstones (Figure 4k,o). In addition, the Fanghushan Formation also records the progressive unroofing history of the Triassic metamorphic bedrock in the Dabie orogen, with sample 21DB47 (stratigraphically higher than sample 21DB50) yielding more Triassic eclogite-facies metamorphic zircon grains (27% vs. 0.5%; Figures 6 and 7a), more Jurassic-Triassic metamafic rutile grains (71% vs. 4%; Figures 6 and 8a), more eclogite-facies garnet (48% vs. 35%; Figure 9d), more mafic garnet (79% vs. 39%; Figure 9e), and higher-pressure phengite (the highest X_{Cel} values (0.30–0.52) are in sample 21DB47 (Mazur et al., 2022, Figure 10d). However, the provenance of the pronounced ca. 1.8 Ga zircon population at the base of the Fanghushan Formation is contentious. Li et al. (2005) interpreted the predominance of the 1.7–1.9 Ga zircons as indicative of a NCC source, because this age is characteristic of the NCC basement. By contrast, Wang et al. (2020) suggested that 1.8–2.0 Ga zircons were sourced from the south from the SuSong Complex in the Dabie orogen, based on the generally similar zircon ages of the Fanghushan Formation gravels and the rocks of the SuSong Complex (Figure 11). Our data support the latter view, particularly because the Fanghushan Formation has abundant Neoproterozoic zircon grains which are unique to the SCB, while the NCC almost entirely lacks zircon of this age. The Triassic metamorphic single-grain ages and the presence of sandstone lithics imply the provenance of the Fanghushan Formation is more likely to be a mixture of Triassic HP-UHP metamorphic rocks and (meta)sedimentary rocks recycled from the Beihuaiyang belt and the SuSong Complex.

In the Nanjing basin, the U–Pb age spectra of detrital zircons and rutile are similar. The metamorphic rutile spectrum is similar to that of the Hefei basin and the peak

at 226 Ma undoubtedly reflects material sourced from the Dabie orogen. The significant ca. 1.8 Ga age populations recorded in both the zircon and rutile spectra are most likely from the Dabie orogen, because there is a small amount of 1.85 Ga metamorphic bedrock in the Dabie orogen itself (Figure 11; Chen et al., 2003; Li et al., 2021; Li, Li, et al., 2004; Li, Zheng, et al., 2004; Wu et al., 2006). Therefore, the provenance of the Zhongshan Formation is almost entirely from the Dabie orogen with some additional recycling of sedimentary rocks resulting in the very high quartz content in these sandstones (Figure 5).

5.1.2 | Huangshi and Yueshan basins

For the Huangshi and Yueshan basins, there are two major questions: whether the Lower Jurassic strata record provenance from the Dabie orogen (e.g. Grimmer et al., 2003; Wang et al., 2009; Yang et al., 2009), and the source of the abundant 1.8 Ga zircon in their basal units (e.g. She et al., 2012; Yang et al., 2010), similar to the contentious ca. 1.8 Ga zircon peak at the base of the Fanghushan Formation.

Concerning the provenance of the Lower Jurassic sediments in the Yueshan and Huangshi basins, She et al. (2012) suggested derivation from a ca. 2000 km long, west-flowing transcontinental palaeoriver with a source in the east Cathaysia Block and an absence of a Dabie orogen provenance signal. This model, termed the Eastern Plateau hypothesis, is based on three arguments including (i) the dominant west- and northwest-directed palaeoflows (present coordinates) measured from tabular cross-beds, (ii) the lack of Triassic metamorphic zircons, and iii) the inference that the 1.86 Ga granites and metamorphic rocks in the Badu Complex in the Wuyi terrane of the Cathaysia Block (Yu et al., 2009, 2010) are the best match for the considerable 1.8 Ga zircon population in the Lower Jurassic sandstones. By contrast, Grimmer et al. (2003) and Wang et al. (2009) emphasise that Triassic detrital phengite (Si > 3.3 pfu) $^{40}Ar/^{39}Ar$ ages from the Lower Jurassic strata could only come from the Dabie orogen, with the orogen providing ca. 50%–80% of the detritus to these basins.

A Dabie orogen source is strongly supported by the data presented here, showing (i) abundant high-grade schist lithics in the Lower Jurassic sandstones calling for a metamorphic source, which is in agreement with the presence of detrital metamorphic garnet (Figure 9) and phengitic mica (Figure 10), and (ii) a latest Permian to Triassic metamorphic rutile U–Pb age population (centered at 251–256 Ma) and minimal 1.8 Ga rutile, which matches with metamorphic bedrock ages in the Dabie orogen (Figures 6 and 11). Notably, the 1.8 Ga zircon population which She et al. (2012) argue as indicating a source in the Badu Complex is not unique (Figure 11), and thus represents an equivocal interpretation. Regarding the paleocurrent data, although this has been corrected for tilt, any subsequent rotation of strata about a vertical axis cannot be excluded. Moreover, the paleocurrent data from the main progradation and the distributary lateral accretion lobes are perpendicular to each other. If not carefully identified as such in the field, these paleocurrent data may lead to erroneous conclusions. Lastly, regional geological data do not support the emergence of an Eastern Plateau as early as Early Jurassic times, as shown by the littoral-shallow sea deposits in the Upper Triassic-Lower Jurassic of eastern China (Kong et al., 2022), and paleoaltimetry evidence for the emergence of Eastern Plateau after the Late Cretaceous with paleoelevations >2 km by 100 Ma (Zhang et al., 2016).

In addition to questioning the existence of an Early Jurassic Eastern Plateau, we also rule out sourcing in the Huangshi and Yueshan basins from the 1.8 Ga Dongling Complex in the Lower Yangtze region immediately east of the Yueshan Basin (Figure 1b) and the southern margin of NCC. This is because (i) the exhumation of the Dongling complex to shallow crustal levels occurred in the Early Cretaceous (Grimmer et al., 2003; Zhu et al., 2007, 2010), and thus postdates the time of sediment deposition and (ii) the Trans-North China Orogen on the southern margin of the NCC was subjected to high-temperature and locally high-pressure granulite-facies conditions at 1.85 Ga (Zhao & Cawood, 2012), which would result in rutile formation; this is clearly recorded in the Carboniferous bauxite deposits of the southern margin of the NCC (Zhao et al., 2021; Zhao & Liu, 2019). Thus, a large amount of 1.85 Ga metamorphic rutile is expected when considering an Upper Palaeozoic source from the southeastern margin of the NCC, but this is not observed (Figures 6 and 11). Additionally, any topographic barrier related to Triassic deep continental subduction would also have blocked transport from the NCC.

Consequently, we suggest the Late Palaeozoic siliciclastic rocks in the Lower Yangtze area to be a more plausible source for 1.7–1.9 Ga zircon population. Detrital zircons from the Permian Longtan Formation in Lower Yangtze area (SCB) exhibit a prominent 1.8 Ga zircon and monazite peak (Kan et al., 2022; Li et al., 2017; Shi et al., 2021; Figure 11), similar to that in the Lower Jurassic strata in this study. Additionally, the Permian strata in the SCB contain abundant chert layers (Kan et al., 2022), which is supported by the abundant chert clasts observed (Figure 4a–f). Recycling is furthermore supported by the high ZTR indices (mean value of 95% for the three samples; Table S1).

In summary, our multi-proxy provenance interpretation of the Huangshi and Yueshan basins implies a

provenance from the Triassic HP-UHP metamorphic rocks of the Dabie orogen and recycling of Permian strata from the Lower Yangtze area of the SCB. Importantly, this provenance and drainage model relies on multiple different provenance tools and shows that detrital zircon U–Pb age spectra alone provide little indication that one of Earth's most significant HP exhumation events was active during the Early Jurassic (cf Grimmer et al., 2003 and this study).

5.2 | Differential exhumation of the Dabie Orogen in the Early Jurassic

Our provenance analysis study shows that rocks of the Dabie orogen, which formed by Triassic continental deep subduction, were exposed to the surface in the Early Jurassic and became source areas to the peripheral basins. However, for each sedimentary basin, can the provenance from the Dabie orogen be constrained accurately enough to trace the exhumation of each tectonic sub-unit or terrane?

The Lower Jurassic Fanghushan Formation in the Hefei basin to the north of the Dabie orogen contains abundant Triassic UHP metamorphic zircons (Li et al., 2005; Wang et al., 2020; this study), which contain coesite, phengite and omphacite inclusions, and a high proportion of eclogite-facies garnet and abundant phengite fragments. Hence, the north side of the Dabie orogen with the deepest crustal HP-UHP gneisses underwent the most exhumation. In contrast, the sedimentary basins on the northeastern, eastern, and southern sides of the Dabie orogen generally lack Triassic metamorphic zircons (Figure 8) but are characterised by Triassic phengite $^{40}Ar/^{39}Ar$ ages (with a main peak at 213–217 Ma; Grimmer et al., 2003) and Triassic rutile U–Pb ages (Figure 6). Most importantly, the main rutile peaks of the Hefei basin (northernmost basin, 216 Ma), Nanjing basin (223 Ma), Yueshan basin (251 Ma), and Huangshi basin (southernmost basin, 256 Ma; Figure 6) mirror the trend of younger metamorphic ages from north to south in the present-day Dabie orogen (Shi et al., 2022). The main rutile U–Pb peak of the Huangshi and Yueshan basins (251–256 Ma) matches with metamorphic zircon ages of the SuSong Complex (259 Ma; Shi et al., 2022), the earliest exhumed HP unit in the Dabie orogen. Similarly, the proportion of metamafic rutile gradually decreases from north to south (Figure 7a), further confirming differential exhumation of the Dabie orogen. The detrital garnet analysis reveals that the Huangshi basin in the south has the largest proportion of amphibolite-facies garnet compared to the Hefei basin in the north, which has the largest proportion of eclogite-facies garnet (Figure 9b,d). This implies lower pressure conditions in the south compared to the north, mimicking the metamorphic facies distribution of the present-day Dabie orogen.

In summary, the Dabie orogen underwent differential uplift and exhumation during the Early Jurassic. The northern margin of the Dabie orogen experienced the most extensive vertical exhumation and denudation. In contrast, the SuSong Complex in the south yields the oldest metamorphic ages that match the main detrital rutile peaks in the Huangshi and Yueshan basins, likely due to its earlier entry into the subduction channel and shallower subduction depths compared to the southern, middle, and northern Dabie terranes. The differential exhumation of the sedimentary basins indicates the Dabie orogen was already a watershed in the Early Jurassic, with the present-day surface tectonic architecture of the Dabie orogen established by the Early Jurassic, except for the subsequent extensive post-orogenic Cretaceous magmatism (see Figs. 12, 13a).

5.3 | Birth of the present-day Dabie Orogen drainage pattern

The more than 380-km-long Dabie orogen, located between the NCC and the SCB, represents the watershed between North and South China, as well as a climatic, geographic and topographic barrier. However, there is little research to date on the initial establishment time of the north–south drainage divide in China and when the Dabie orogen first became that watershed.

The drainage evolution of the large Chinese river systems has received significant attention, especially the birth of the modern Yangtze River (e.g. Zheng et al., 2013). Our detailed source-to-sink system reconstruction of the Early Jurassic basins peripheral to the Dabie orogen provide a valuable reference framework for the drainage evolution of these large rivers. At present, the northern Dabie terrane has the highest elevation (max elevation: 1729 m) (Figure 1b), and the provenance of the Hefei basin is mainly from the northern Dabie terrane. The sedimentary basins on the eastern side of the orogen received detritus from the east/northeast-flowing river systems of the northern and central Dabie terranes, and the sedimentary basins on the southern side received detritus flowing south across the southern Dabie terrane and the SuSong Complex. These north-flowing branches originating from the Dabie orogen may have merged into an ancient Huai River, and the south- and east-flowing branches may coincide with the modern tributaries in the Dabie orogen (i.e. Qishui, Xishui, Bashui, Jushui, Sheshui, Huanshui, Qianshui, Er'lang river, Wan river, Bonian river, Figure 13), presently coalesce into the Middle-Lower Yangtze River. Hence, we suggest that

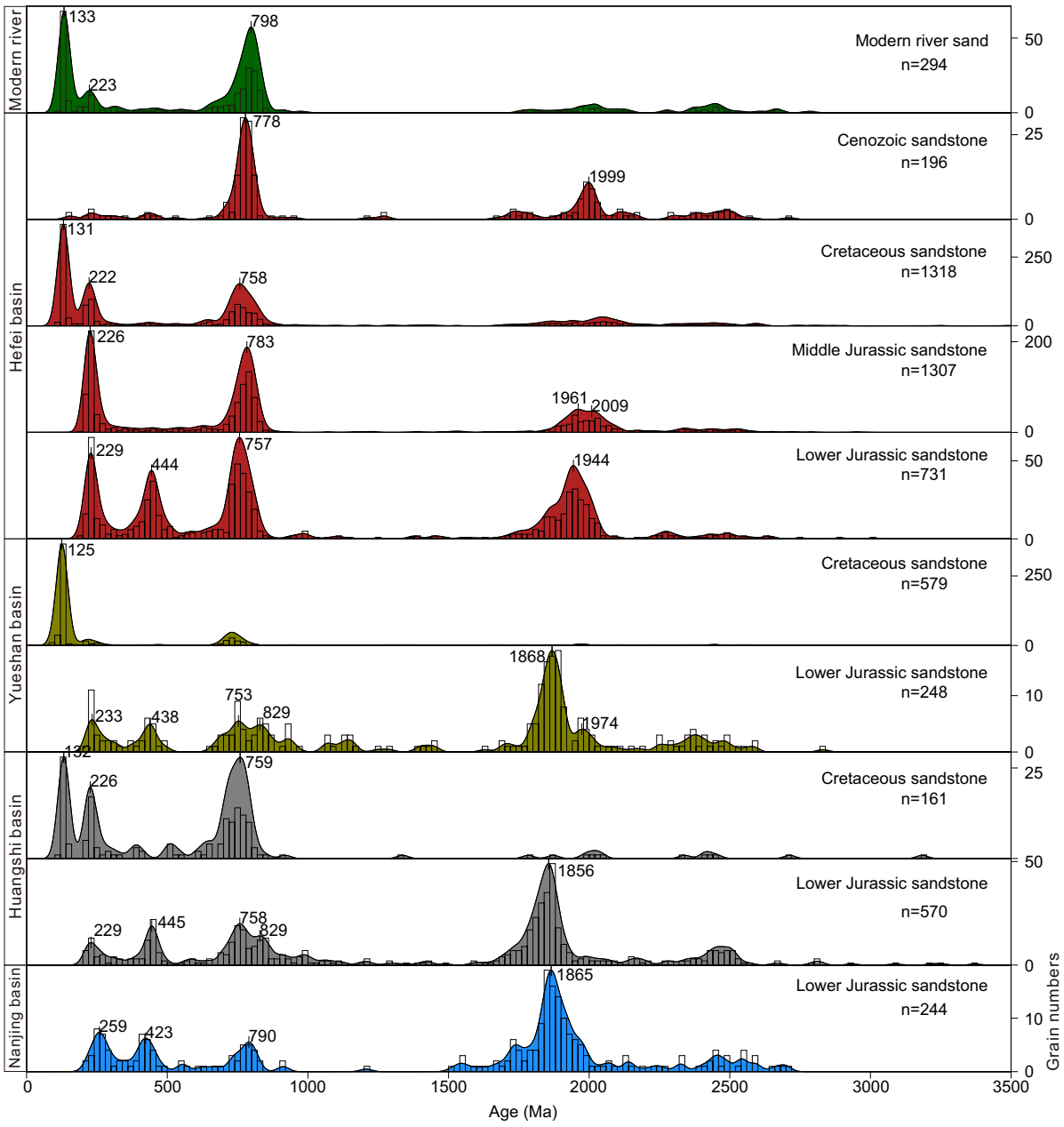

FIGURE 12 Compiled detrital zircon data from sedimentary basins constraining the drainage development history since the Early Jurassic. Data from modern river sands derived from the Dabie orogen according to Lin et al. (2022). Data sources for the Hefei basin: Middle Jurassic (Wang et al., 2019, 2021; Zhu, Liang, et al., 2017; Zhu, Wang, et al., 2017), Cretaceous (Wang et al., 2021; Yang et al., 2022; Zhu, Liang, et al., 2017; Zhu, Wang, et al., 2017), Cenozoic (Yang et al., 2022). Cretaceous sandstones from the Huangshi basin are from Zhao et al. (2022) and from Wang et al. (2023) for the Yueshan Basin. All ages are displayed on the KDEs and histograms with a 20 Ma KDE bandwidth.

Dabie orogen had an Early Jurassic watershed and drainage pattern similar to today (Figure 13b,c), even if the current drainage pattern of the major rivers such as the Yangtze River and Huai River potentially initiated as late as the Late Cenozoic (Zheng et al., 2021).

Comparing the detrital zircon spectra compiled from various sedimentary basins in the region, it is found that the drainage pattern of the Dabie orogen (established in the Early Jurassic) has undergone significant modification since the Cretaceous. The Cretaceous intrusions and migmatites in the Dabie orogen indicate significant exhumation of presently exposed (U)HP-rocks from mid-crustal levels (Ratschbacher et al., 2000). Early Cretaceous granites in the Dabie orogen contributed erosional material to the Cretaceous sandstones of the Yueshan, Huangshi and Hefei basins (Figure 12), and the detrital zircon spectra of modern river sands (Lin et al., 2022) record detritus from the Dabie orogen, including the Early Cretaceous granites,

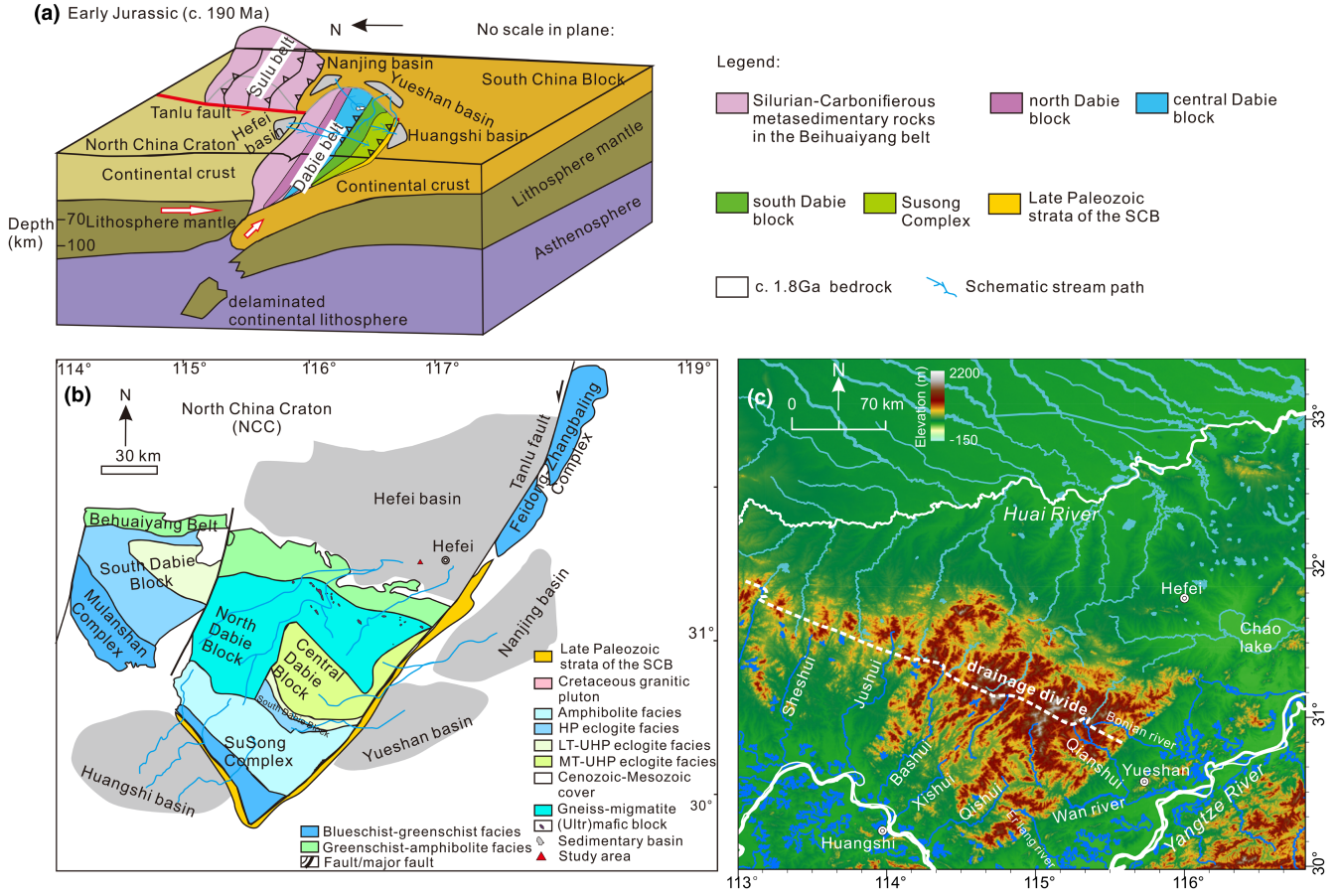

FIGURE 13 Schematic model of the Early Jurassic Dabie orogen. (a) 3D tectonic reconstruction of exhumed tectonometamorphic units and the location of peripheral sedimentary basins. Note, the evolutionary history of the Sulu orogen is not emphasised in this model. (b) Reconstruction of the palaeo-drainage pattern. (c) Present-day drainage pattern for comparison.

Triassic metamorphic rocks and their Neoproterozoic protoliths. Given these observations, we suggest that the extensive post-collisional magmatic events in the Cretaceous and rapid exhumation since the Cenozoic (Ding et al., 2021) has triggered drainage expansion and the onset of more extensive surface denudation of the high topography and relief of the Dabie orogen. However, the drainage area and drainage divide of these sedimentary basins has not changed, as they are all derived from the Dabie orogen. We therefore emphasise here that the watershed of Dabie orogenic belt was born in the Early Jurassic.

It should be noted that exhumation and growth of the Dabie orogen did not result in substantial topographic relief during the Early Jurassic and thus did not significantly divide the climate of North and South China. In the Early Jurassic, both North and South China were located in the Boreotropical climate zone, and extensive coal seams developed in both these regions at the same time (Boucot et al., 2013; Figure 13). Therefore, the formation of the Qinling-Tongbai-Dabie line as a major climate and geomorphic boundary between North and South China may have taken place later than the Early Jurassic, probably during the subsequent Cretaceous to Cenozoic extensional tectonism which affected and shaped the Dabie orogen significantly (Ding et al., 2021; Grimmer et al., 2002; Ratschbacher et al., 2000). Nevertheless, Early Jurassic exhumation of the Dabie Orogen marks the birth of the embryonic drainage systems of East China, namely, the watersheds of the Huai River to the north and the tributary systems (i.e. Qishui, Xishui, Bashui, Qianshui, etc) to the south. With the emergence of fully connected, throughgoing major river systems, these rivers were eventually primed to develop into their present-day drainage systems.

6 | CONCLUSIONS

Using a multi-proxy provenance dataset from the sandstones of the Early Jurassic sedimentary basin that border the Dabie orogen, we shed new light on provenance linkages and paleogeographic-drainage models for the Dabie orogen.

High-grade schist lithics and muscovite grains, abundant metamorphic garnet and phengite, and main rutile U–Pb

peaks of 216–256 Ma (with older peaks in basins towards the south) indicate a source from the Triassic HP-UHP belts in the Dabie orogen. Sedimentary lithics (sandstone and chert) and ultra-stable heavy-mineral assemblages indicate recycling and the contribution of an additional source, most likely Permian strata of the SCB. The Triassic HP-UHP rocks were first exposed on Earth's surface in the Early Jurassic. The combination of rutile U–Pb ages and multiple single-grain geochemistry tools, which indicate variable grades and compositions for the metamorphic source rocks in the different basins, implies a differential exhumation history of the Dabie orogen in the Early Jurassic. Thus, the present surface tectonic architecture of the Dabie orogen was already established in the Early Jurassic, with the exception of subsequent Cretaceous plutonism. Consequently, Early Jurassic exhumation of the Dabie orogen marked the initial development of the watershed between Northern and Southern China.

ACKNOWLEDGEMENTS

The authors are grateful to Prof. Dr. Atle Rotevatn for the editorial handling of this manuscript and two anonymous reviewers for their constructive reviews and helpful suggestions that greatly improved the manuscript. This work was funded by NSFC project (42050102, 41888101) awarded to X.H. D.C. acknowledges support from the Science Foundation Ireland (SFI) through research grants 12/IP/1663, 13/RC/2092 and 13/RC/2092_P2, and 15/IA/3024.

CONFLICT OF INTEREST STATEMENT

We declare that there is no conflict of interest in the submission of this manuscript, and all authors have approved its submission.

DATA AVAILABILITY STATEMENT

The data that support the findings of this study are available from the corresponding author upon reasonable request.

ORCID

Xiumian Hu https://orcid.org/0000-0002-5401-8682
David Chew https://orcid.org/0000-0002-6940-1035
Jan Schönig https://orcid.org/0000-0001-9296-7582
Wendong Liang https://orcid.org/0000-0003-2704-0996
Foteini Drakou https://orcid.org/0000-0001-6618-4541

REFERENCES

Baldwin, S. L., Schönig, J., Gonzalez, J. P., Davies, H., & von Eynatten, H. (2021). Garnet sand reveals rock recycling processes in the youngest exhumed high-and ultrahigh-pressure terrane on earth. *Proceedings of the National Academy of Sciences*, *118*(3), e2017231118.

Boucot, A. J., Xu, C., Scotese, C. R., & Morley, R. J. (2013). Phanerozoic paleoclimate: An atlas of lithologic indicators of climate, Society of Economic Paleontologists and Mineralogists (Society for Sedimentary Geology).

Bureau of Geology and Mineral Resources of Anhui Province, Regional Geology of Anhui Province, People's Republic of China, Ministry of Geology and Mineral Resources. (1987). Geological Memoirs, Series 1, No. 5. Beijing: Geological Publishing House (pp. 150–152) (in Chinese).

Calvet, M., Gunnell, Y., & Laumonier, B. (2021). Denudation history and palaeogeography of the Pyrenees and their peripheral basins: An 84-million-year geomorphological perspective. *Earth-Science Reviews*, *215*, 103436. https://doi.org/10.1016/j.earscirev.2020.103436

Canil, D., Mihalynuk, M., & Charnell, C. (2006). Sedimentary record for exhumation of ultrahigh pressure (UHP) rocks in the northern cordillera, British Columbia, Canada. *Geological Society of America Bulletin*, *118*(9–10), 1171–1184.

Cao, Z. Y. (2000). Some specimens of gymnospermae from the lower part of Xiangshan Group in Jiangsu and Anhui Provinces with study on their cuticules. *Acta Micropalaeontologica Sinica*, *3*, 334–338.

Chen, D., Deloule, E., Cheng, H., Xia, Q., & Wu, Y. (2003). Preliminary study of microscale zircon oxygen isotopes for Dabie-Sulu metamorphic rocks: Ion probe in situ analyses. *Chinese Science Bulletin*, *48*, 1670–1678.

Chen, T. N., Chen, R. X., Zheng, Y. F., Zhou, K., Yin, Z. Z., Wang, Z. M., Gong, B., & Zha, X. P. (2022). The effect of supercritical fluids on Nb-Ta fractionation in subduction zones: Geochemical insights from a coesite-bearing eclogite-vein system. *Geochimica et Cosmochimica Acta*, *335*, 23–55.

Chen, Z., & Li, Q. (2008). Zr-in-rutile thermometry in eclogite at Jinheqiao in the Dabie orogen and its geochemical implications. *Chinese Science Bulletin*, *53*(5), 768–776.

Chen, Z., Zhou, J., Li, R., & Wan, Y. (2005). Mineral inclusions and internal structure of detrital zircons from lower Jurassic sedimentary rocks of Fanghushan formation in Hefei Basin. *Acta Mineralogica Sinica*, *25*(1), 89–96.

Chen, Z. H., & Xing, G. F. (2016). Geochemical and zircon U–Pb–Hf–O isotopic evidence for a coherent Paleoproterozoic basement beneath the Yangtze block, South China. *Precambrian Research*, *279*, 81–90.

Cheng, H., & Vervoort, J. D. (2015). Combined geochemistry and geochronology constrains coupled subduction of oceanic and continental crust in the Huwan shear zone, Central China. *American Mineralogist*, *100*(1), 181–194.

Cheng, H., Zhang, C., Vervoort, J. D., Wu, Y., Zheng, Y., Zheng, S., & Zhou, Z. (2011). New Lu–Hf geochronology constrains the onset of continental subduction in the Dabie orogen. *Lithos*, *121*(1–4), 41–54.

Chew, D., O'Sullivan, G., Caracciolo, L., Mark, C., & Tyrrell, S. (2020). Sourcing the sand: Accessory mineral fertility, analytical and other biases in detrital U−Pb provenance analysis. *Earth-Science Reviews*, *202*, 103093.

Chew, D., Petrus, J., & Kamber, B. (2014). U–Pb LA–ICPMS dating using accessory mineral standards with variable common Pb. *Chemical Geology*, *363*, 185–199.

Chew, D. M., Sylvester, P. J., & Tubrett, M. N. (2011). U–Pb and Th–Pb dating of apatite by LA-ICPMS. *Chemical Geology*, *280*(1–2), 200–216.

Coggon, R., & Holland, T. (2002). Mixing properties of phengitic micas and revised garnet-phengite thermobarometers. *Journal of Metamorphic Geology*, *20*(7), 683–696.

Di Capua, A., Barilaro, F., & Groppelli, G. (2021). Deep-water accumulation of Volcaniclastic detritus from a petrographic point of view: Beginning a Discussion from the alpine peripheral basins. *Geosciences*, *11*(11), 441. https://doi.org/10.3390/geosciences11110441

Ding, R., Chang, Y., Min, K., Xu, C., & Wang, W. (2021). Post-orogenic topographic evolution of the Dabie orogen, eastern China: Insights from apatite and zircon (U-Th)/He thermochronology. *Geomorphology*, *374*, 107487. https://doi.org/10.1016/j.geomorph.2020.107487

Fan, W. M., Guo, F., Wang, Y. J., & Zhang, M. (2004). Late Mesozoic volcanism in the northern Huaiyang tectono-magmatic belt, Central China: Partial melts from a lithospheric mantle with subducted continental crust relicts beneath the Dabie orogen? *Chemical Geology*, *209*(1–2), 27–48.

Franz, L., Romer, R. L., Klemd, R., Schmid, R., Oberhansli, R., Wagner, T., & Shuwen, D. (2001). Eclogite-facies quartz veins within metabasites of the Dabie Shan (eastern China): Pressure-temperature-time-deformation path, composition of the fluid phase and fluid flow during exhumation of high-pressure rocks. *Contributions to Mineralogy and Petrology*, *141*(3), 322–346.

Gao, C., Liu, Y., Zong, K., Hu, Z., & Gao, S. (2010). Microgeochemistry of rutile and zircon in eclogites from the CCSD main hole: Implications for the fluid activity and thermo-history of the UHP metamorphism. *Lithos*, *115*(1–4), 51–64.

Gao, X. Y., Zheng, Y. F., & Chen, Y. X. (2011). U-Pb ages and trace elements in metamorphic zircon and titanite from UHP eclogite in the Dabie orogen: Constraints on P-T-t path. *Journal of Metamorphic Geology*, *29*(7), 721–740.

Gao, X. Y., Zheng, Y. F., Xia, X. P., & Chen, Y. X. (2014). U–Pb ages and trace elements of metamorphic rutile from ultrahigh-pressure quartzite in the Sulu orogen. *Geochimica et Cosmochimica Acta*, *143*, 87–114.

Garzanti, E. (2019). Petrographic classification of sand and sandstone. *Earth-Science Reviews*, *192*, 545–563.

Garzanti, E., & Andò, S. (2019). Heavy minerals for junior woodchucks. *Minerals*, *9*(3), 148.

Grimmer, J. C., Jonckheere, R., Enkelmann, E., Ratschbacher, L., Hacker, B. R., Blythe, A. E., Wagner, G. A., Wu, Q., Liu, S., & Dong, S. (2002). Cretaceous—Cenozoic history of the southern Tan-Lu fault zone: Apatite fission-track and structural constraints from the Dabie Shan (eastern China). *Tectonophysics*, *359*(3), 225–253. https://doi.org/10.1016/S0040-1951(02)00513-9

Grimmer, J. C., Ratschbacher, L., McWilliams, M., Franz, L., Gaitzsch, I., Tichomirowa, M., Hacker, B. R., & Zhang, Y. (2003). When did the ultrahigh-pressure rocks reach the surface? A 207Pb/206Pb zircon, 40Ar/39Ar white mica, Si-in-white mica, single-grain provenance study of Dabie Shan synorogenic foreland sediments. *Chemical Geology*, *197*(1–4), 87–110.

Guo, B. (1984). The sedimentary environment of Mesozoic coal measures along the Changjiang River in Anhui Province. *Journal of Huainan Institute of Mining*, *3*, 44–65.

Guo, G., Jia, G., Xu, S., Zhang, X., & Sun, X. X. (2014). Sequence division and sedimentary facies evolution analysis of the middle-early Jurassic, Xiangshan Group in Ningwu and Lishui, Jiangsu Province. *Geological Science and Technology Information*, *33*(6), 39–45.

Guo, S., Tang, P., Su, B., Chen, Y., Ye, K., Zhang, L., Gao, Y., Liu, J., & Yang, Y. (2017). Unusual replacement of Fe-Ti oxides by rutile during retrogression in amphibolite-hosted veins (Dabie UHP terrane): A mineralogical record of fluid-induced oxidation processes in exhumed UHP slabs. *American Mineralogist*, *102*(11), 2268–2283.

Guo, S., Ye, K., Chen, Y., Liu, J., Mao, Q., & Ma, Y. (2012). Fluid–rock interaction and element mobilization in UHP metabasalt: Constraints from an omphacite–epidote vein and host eclogites in the Dabie orogen. *Lithos*, *136*, 145–167.

Hacker, B. R., Ratschbacher, L., Webb, L., McWilliams, M. O., Ireland, T., Calvert, A., Dong, S., Wenk, H. R., & Chateigner, D. (2000). Exhumation of ultrahigh-pressure continental crust in east Central China: Late Triassic-early Jurassic tectonic unroofing. *Journal of Geophysical Research: Solid Earth*, *105*(B6), 13339–13364. https://doi.org/10.1029/2000JB900039

Hacker, B. R., & Wang, Q. (1995). Ar/Ar geochronology of ultrahigh-pressure metamorphism in Central China. *Tectonics*, *14*(4), 994–1006.

Hart, E., Storey, C., Bruand, E., Schertl, H. P., & Alexander, B. D. (2016). Mineral inclusions in rutile: A novel recorder of HP-UHP metamorphism. *Earth and Planetary Science Letters*, *446*, 137–148.

Hong, Y. C. (1986). Early Jurassic fossil insects from Daye of Hubei Province. *Proceedings on Stratigraphic Palaeontology*, *2*, 181–189.

Hoskin, P. W., & Schaltegger, U. (2003). The composition of zircon and igneous and metamorphic petrogenesis. *Reviews in Mineralogy and Geochemistry*, *53*(1), 27–62.

Hou, C., Yang, T., & Shi, Y. (2016). In-situ SHRIMP U—Pb dating of Rutiles in Eclogite from Dabie UHP Metamorphic Belt and its geochronological significance. *Journal of Earth Sciences and Environment*, *38*(3), 334–340.

Hou, X., Yu, Z., Chen, S., Liu, L., & Xiao, Y. (2022). Trace element mobility in subducted marble and associated eclogite: Constraints from UHP rocks in the Shuanghe area, central-East China. *Journal of Earth Science* https://kns.cnki.net/kcms/detail/42.1788.P.20220609.1514.004.html

Hou, Z., Xiao, Y., Shen, J., & Yu, C. (2020). In situ rutile U—Pb dating based on zircon calibration using LA-ICP-MS, geological applications in the Dabie orogen, China. *Journal of Asian Earth Sciences*, *192*, 104261.

Huang, D. (2019). Jurassic integrative stratigraphy and timescale of China. *Science China Earth Sciences*, *62*, 223–255.

Huang, D., Fang, Y., Li, J., & Li, X. (2021). Lithostratigraphic subdivision and correlation of the Jurassic in China. *Journal of Stratigraphy*, *45*(3), 364–374. https://doi.org/10.19839/j.cnki.dcxzz.2021.0029

Huang, J., Xiao, Y., Gao, Y., Hou, Z., & Wu, W. (2012). Nb–Ta fractionation induced by fluid-rock interaction in subduction-zones: Constraints from UHP eclogite-and vein-hosted rutile from the Dabie orogen, Central-Eastern China. *Journal of Metamorphic Geology*, *30*(8), 821–842.

Huang, P. (2000). Discovery of middle Jurassic palynological assemblage from Beixiangshan of Nanjing. *Acta Micropalaeontologica Sinica*, *4*, 457–506.

Huang, Q. (1983). The early Jurassic Xiangshan flora from the Yangzi River valley in Anhui Province of eastern China. *Earth Science-Journal of China University of Geosciences*, *8*(2), 25–36.

Huang, Q. (1988). Vertical diversities of the early Jurassic plant fossils in the middle-lower Changjiang Valley. *Geological Review*, *34*(3), 193–294.

Huang, Q., & Lu, Z. (1988). The early Jurassic Wuchang flora from Southeast Hubei Province. *Earth Science-Journal of China University of Geosciences*, *13*(5), 545–552.

Hubert, J. F. (1962). A zircon-tourmaline-rutile maturity index and the interdependence of the composition of heavy mineral assemblages with the gross composition and texture of sandstones. *Journal of Sedimentary Research*, *32*(3), 440–450.

Ingersoll, R. V., Bullard, T. F., Ford, R. L., Grimm, J. P., Pickle, J. D., & Sares, S. W. (1984). The effect of grain size on detrital modes: A test of the Gazzi-Dickinson point-counting method. *Journal of Sedimentary Research*, *54*(1), 103–116.

Jackson, S. E., Pearson, N. J., Griffin, W. L., & Belousova, E. A. (2004). The application of laser ablation-inductively coupled plasma-mass spectrometry to in situ U–Pb zircon geochronology. *Chemical Geology*, *211*(1–2), 47–69.

Jahn, B. M., Rumble, D., & Liou, J. G. (2003). Geochemistry and isotope tracer study of UHP metamorphic rocks. In D. A. Carswell & R. Compagnoni (Eds.), *Ultrahigh pressure metamorphism* (Vol. *5*, pp. 365–414). EMU Notes in Mineralogy.

Ju, K. X. (1987). Subdivision of the lower-middle Jurassic strata in South Jiangsu. *Bulletin of Nanjing Institute of Geology and Mineral Resources, Chinese Academy of Geological Sciences*, *4*, 33–44.

Kan, T., Li, L., Chen, M., Liu, H., Zhao, X., Jiang, R., & Han, X. (2022). Provenance of the siliciclastic rocks in the lower Yangtze region: Implications for Paleozoic tectonic switching of the northeastern South China block. *Journal of Asian Earth Sciences*, *228*, 105145.

Kirkland, C., Smithies, R., Taylor, R., Evans, N., & McDonald, B. (2015). Zircon Th/U ratios in magmatic environs. *Lithos*, *212*, 397–414.

Kohn, M. J. (2020). A refined zirconium-in-rutile thermometer. *American Mineralogist: Journal of Earth and Planetary Materials*, *105*(6), 963–971.

Kong, J. T., Xu, Z. J., Tao, G. Z., Cheng, R. H., & Wang, L. L. (2022). U–Pb geochronology of upper Triassic – Lower Jurassic detrital sequences from SE margin of the South China block: Implications for Palaeo-Pacific subduction and tectonic evolution. *Geological Magazine*, *159*(6), 833–852.

Kylander-Clark, A. R., Hacker, B. R., & Mattinson, C. G. (2012). Size and exhumation rate of ultrahigh-pressure terranes linked to orogenic stage. *Earth and Planetary Science Letters*, *321*, 115–120.

Li, C., & Hu, X. M. (2022). The earliest denudation record of the Dabie Orogenic Belt evidenced from the middle Triassic Huangmaqing formation in the Ningwu Basin. *Geological Journal of China Universities*, *28*(4), 527–538. (in Chinese with English abstract).

Li, C., Lü, X., Hu, X. M., Yu, J. H., & Sun, G. Y. (2017). Sandstone memory of a late Paleozoic continental arc in Southeast China (lower Yangtze region). *Chinese Science Bulletin*, *62*(25), 2951–2966.

Li, M., Hinnov, L., & Kump, L. (2019). Acycle: Time-series analysis software for paleoclimate research and education. *Computers & Geosciences*, *127*, 12–22.

Li, Q., Li, S., Zheng, Y. F., Li, H., Massonne, H. J., & Wang, Q. (2003). A high precision U–Pb age of metamorphic rutile in coesite-bearing eclogite from the Dabie Mountains in Central China: A new constraint on the cooling history. *Chemical Geology*, *200*(3–4), 255–265.

Li, R., Li, Z., Jiang, M., Sun, S., Jin, F., & Zhang, W. (2000). Compositions of Jurassic detrital garnets in Hefei Basin and its implication to provenance reconstruction and stratigraphic correlation. *Science in China Series D: Earth Sciences*, *43*, 167–177.

Li, R., Wan, Y., Cheng, Z., Zhou, J., Li, S., Jin, F., Meng, Q., Li, Z., & Jiang, M. (2005). Provenance of Jurassic sediments in the Hefei Basin, east-Central China and the contribution of high-pressure and ultrahigh-pressure metamorphic rocks from the Dabie Shan. *Earth and Planetary Science Letters*, *231*(3–4), 279–294.

Li, S., Xiao, Y., Liou, D., Chen, Y., Ge, N., Zhang, Z., Sun, S. S., Cong, B., Zhang, R., & Hart, S. R. (1993). Collision of the North China and Yangtse blocks and formation of coesite-bearing eclogites: Timing and processes. *Chemical Geology*, *109*(1–4), 89–111.

Li, S. Q., Schmitt, A. K., & Chen, F. (2021). Early cretaceous mafic–intermediate dykes in the Dabie orogen as indicators for post-collisional lithosphere removal. *Lithos*, *388*, 106065.

Li, X. P., Zheng, Y. F., Wu, Y. B., Chen, F., Gong, B., & Li, Y. L. (2004). Low-T eclogite in the Dabie terrane of China: Petrological and isotopic constraints on fluid activity and radiometric dating. *Contributions to Mineralogy and Petrology*, *148*, 443–470.

Li, Z., Li, R., Sun, S., & Wang, Q. (2004). Jurassic depositional records and sandstone provenances in Hefei Basin, Central China: Implication for Dabie orogenesis. *Island Arc*, *13*(2), 346–358.

Li, Z., Li, R., Sun, S., & Zhang, W. (2003). Mesozoic basin-fill records in south foot of the Dabie Mountains: Implication for Dabie orogenic attributes. *Science in China Series D: Earth Sciences*, *46*(3), 217–230.

Li, Z., Sun, S., Li, R., & Jiang, M. (2001). Mesozoic fill-sequences in Hefei basin: Implication for Dabie orogenesis, Central China. *Science in China Series D: Earth Sciences*, *44*(1), 52–63.

Liang, J., Ding, X., Sun, X., Zhang, Z., Zhang, H., & Sun, W. (2009). Nb/Ta fractionation observed in eclogites from the Chinese continental scientific drilling project. *Chemical Geology*, *268*(1–2), 27–40.

Lin, X., Wu, Z., Zhao, X., Zhang, Y., Chen, J., & Liu, H. (2022). Detrital zircon U-Pb age characteristics of Main Rivers around Jianghan Basin and implications of provenance tracing. *Acta Geoscientica Sinica*, *43*(1), 73–81. https://doi.org/10.3975/cagsb.2021.091701

Liou, J., Ernst, W., Zhang, R., Tsujimori, T., & Jahn, B. (2009). Ultrahigh-pressure minerals and metamorphic terranes–The view from China. *Journal of Asian Earth Sciences*, *35*(3–4), 199–231.

Liu, F., Gerdes, A., Liou, J., Xue, H., & Liang, F. (2006). SHRIMP U-Pb zircon dating from Sulu-Dabie dolomitic marble, eastern China: Constraints on prograde, ultrahigh-pressure and retrograde metamorphic ages. *Journal of Metamorphic Geology*, *24*(7), 569–589.

Liu, J., Ye, K., Maruyama, S., Cong, B., & Fan, H. (2001). Mineral inclusions in zircon from gneisses in the ultrahigh-pressure zone of the Dabie Mountains, China. *The Journal of Geology*, *109*(4), 523–535.

Liu, L., Xiao, Y., Aulbach, S., Li, D., & Hou, Z. (2014). Vanadium and niobium behavior in rutile as a function of oxygen fugacity: Evidence from natural samples. *Contributions to Mineralogy and Petrology*, *167*, 1–22.

Liu, L., Xiao, Y., Wörner, G., Kronz, A., Simon, K., & Hou, Z. (2014). Detrital rutile geochemistry and thermometry from the Dabie orogen: Implications for source–sediment links in a UHPM terrane. *Journal of Asian Earth Sciences*, *89*, 123–140.

Liu, S., Heller, P. L., & Zhang, G. (2003). Mesozoic basin development and tectonic evolution of the Dabieshan orogenic belt, Central China. *Tectonics*, *22*(4), 1038. https://doi.org/10.1029/2002TC001390

Liu, S., Steel, R., & Zhang, G. (2005). Mesozoic sedimentary basin development and tectonic implication, northern Yangtze block, eastern China: Record of continent–continent collision. *Journal of Asian Earth Sciences*, *25*(1), 9–27. https://doi.org/10.1016/j.jseaes.2004.01.010

Liu, S., & Zhang, G. (2013). Mesozoic basin development and its indication of collisional orogeny in the Dabie orogen. *Chinese Science Bulletin*, *58*, 827–852.

Liu, S., Zhang, G., Ritts, B. D., Zhang, H., Gao, M., & Qian, C. (2010). Tracing exhumation of the Dabie Shan ultrahigh-pressure metamorphic complex using the sedimentary record in the Hefei Basin, China. *Bulletin*, *122*(1–2), 198–218.

Liu, X., Jahn, B. M., Dong, S., Lou, Y., & Cui, J. (2008). High-pressure metamorphic rocks from Tongbaishan, Central China: U–Pb and 40Ar/39Ar age constraints on the provenance of protoliths and timing of metamorphism. *Lithos*, *105*(3–4), 301–318.

Locock, A. J. (2008). An excel spreadsheet to recast analyses of garnet into end-member components, and a synopsis of the crystal chemistry of natural silicate garnets. *Computers & Geosciences*, *34*(12), 1769–1780.

Lu, W., Li, Y., Zhou, G., Chen, C., Yao, G., Shen, Y., Cao, Z., Lin, Q., & Li, W. (1985). The Jurassic system in Chaohu, Anhui Province. *Journal of Stratigraphy*, *9*(3), 180–185.

Luvizotto, G., Zack, T., Meyer, H., Ludwig, T., Triebold, S., Kronz, A., Münker, C., Stockli, D., Prowatke, S., & Klemme, S. (2009). Rutile crystals as potential trace element and isotope mineral standards for microanalysis. *Chemical Geology*, *261*(3–4), 346–369.

Mazur, S., Majka, J., Barnes, C. J., McClelland, W., Bukała, M., Janák, M., & Kośmińska, K. (2022). Exhumation of the high-pressure Richarddalen complex in NW Svalbard: Insights from 40Ar/39Ar geochronology. *Terra Nova*, *34*(4), 330–339.

Meng, Q. R., Li, S. Y., & Li, R. W. (2007). Mesozoic evolution of the Hefei basin in eastern China: Sedimentary response to deformations in the adjacent Dabieshan and along the Tanlu fault. *Geological Society of America Bulletin*, *119*(7–8), 897–916.

Meng, Q. R., Wu, G. L., Fan, L. G., & Wei, H. H. (2019). Tectonic evolution of early Mesozoic sedimentary basins in the North China block. *Earth-Science Reviews*, *190*, 416–438. https://doi.org/10.1016/j.earscirev.2018.12.003

Morton, A. C., & Hallsworth, C. (1994). Identifying provenance-specific features of detrital heavy mineral assemblages in sandstones. *Sedimentary Geology*, *90*(3–4), 241–256.

Okay, A. I., Xu, S., & Sengor, A. C. (1989). Coesite from the Dabie Shan eclogites, Central China. *European Journal of Mineralogy*, *1*(4), 595–598.

Paton, C., Hellstrom, J., Paul, B., Woodhead, J., & Hergt, J. (2011). Iolite: Freeware for the visualisation and processing of mass spectrometric data. *Journal of Analytical Atomic Spectrometry*, *26*(12), 2508–2518.

Peng, P., Mitchell, R. N., & Chen, Y. (2022). Earth's one-of-a-kind fault: The Tanlu fault. *Terra Nova*, *34*(5), 381–394. https://doi.org/10.1111/ter.12611

Pereira, I., & Storey, C. D. (2023). Detrital rutile: Records of the deep crust, ores and fluids. *Lithos*, 438–439, 107010.

Petrus, J. A., & Kamber, B. S. (2012). VizualAge: A novel approach to laser ablation ICP-MS U-Pb geochronology data reduction. *Geostandards and Geoanalytical Research*, *36*(3), 247–270.

Ratschbacher, L., Hacker, B. R., Calvert, A., Webb, L. E., Grimmer, J. C., McWilliams, M. O., Ireland, T., Dong, S., & Hu, J. (2003). Tectonics of the Qinling (Central China): Tectonostratigraphy, geochronology, and deformation history. *Tectonophysics*, *366*(1), 1–53. https://doi.org/10.1016/S0040-1951(03)00053-2

Ratschbacher, L., Hacker, B. R., Webb, L. E., McWilliams, M., Ireland, T., Dong, S., Calvert, A., Chateigner, D., & Wenk, H. R. (2000). Exhumation of the ultrahigh-pressure continental crust in east Central China: Cretaceous and Cenozoic unroofing and the Tan-Lu fault. *Journal of Geophysical Research: Solid Earth*, *105*(B6), 13303–13338. https://doi.org/10.1029/2000JB900040

Rubatto, D. (2017). Zircon: The metamorphic mineral. *Reviews in Mineralogy and Geochemistry*, *83*(1), 261–295.

Sassi, R., Harte, B., Carswell, D., & Yujing, H. (2000). Trace element distribution in Central Dabie eclogites. *Contributions to Mineralogy and Petrology*, *139*, 298–315.

Schmidt, A., Weyer, S., John, T., & Brey, G. P. (2009). HFSE systematics of rutile-bearing eclogites: New insights into subduction zone processes and implications for the earth's HFSE budget. *Geochimica et Cosmochimica Acta*, *73*(2), 455–468.

Schmitt, A. K., & Zack, T. (2012). High-sensitivity U–Pb rutile dating by secondary ion mass spectrometry (SIMS) with an O2+ primary beam. *Chemical Geology*, *332*, 65–73.

Schönig, J., Meinhold, G., von Eynatten, H., & Lünsdorf, N. K. (2018). Tracing ultrahigh-pressure metamorphism at the catchment scale. *Scientific Reports*, *8*(1), 2931.

Schönig, J., von Eynatten, H., Meinhold, G., & Lünsdorf, N. K. (2019). Diamond and coesite inclusions in detrital garnet of the Saxonian Erzgebirge, Germany. *Geology*, *47*(8), 715–718.

Schönig, J., von Eynatten, H., Meinhold, G., & Lünsdorf, N. K. (2022). The sedimentary record of ultrahigh-pressure metamorphism: A perspective review. *Earth-Science Reviews*, *227*, 103985.

Schönig, J., von Eynatten, H., Tolosana-Delgado, R., & Meinhold, G. (2021). Garnet major-element composition as an indicator of host-rock type: A machine learning approach using the random forest classifier. *Contributions to Mineralogy and Petrology*, *176*, 1–21.

Sharman, G. R., Sharman, J. P., & Sylvester, Z. (2018). detritalPy: A python-based toolset for visualizing and analysing detrital geo-thermochronologic data. *The Depositional Record*, *4*(2), 202–215.

She, Z., Ma, C., Wan, Y., Zhang, J., Li, M., Chen, L., Xu, W., Li, Y., Ye, L., & Gao, J. (2012). An early Mesozoic transcontinental palaeoriver in South China: Evidence from detrital zircon U–Pb geochronology and Hf isotopes. *Journal of the Geological Society*, *169*(3), 353–362.

Shen, J. (2013). Common Pb isotope mapping of Dabie UHPM zones and trace element geochemistry of eclogites and rutiles (PhD thesis). University of Science and Technology of China.

Shi, G., Huang, C., Xu, S., Ge, W., Zhang, Y., & Shi, W. (2021). Source to sink systems of the upper permian longtan formation in the lower yangtze region, China: New insights from detrital

monazite U–Pb ages and heavy mineral chemistry. *Marine and Petroleum Geology*, *126*, 104928.

Shi, Y., Liu, X., La, X., Peng, C., Hou, Z., Zhou, A., & Wang, J. (2022). Tectonic evolution of the southern Dabie Orogenic Belt, China: Insights from peak P–T conditions and U–Pb zircon dating of the Susong metamorphic complex. *Minerals*, *12*(10), 1201.

Stacey, J. T., & Kramers, J. D. (1975). Approximation of terrestrial lead isotope evolution by a two-stage model. *Earth and Planetary Science Letters*, *26*(2), 207–221.

Sun, S. S., & McDonough, W. F. (1989). Chemical and isotopic systematics of oceanic basalts: Implications for mantle composition and processes. *Geological Society, London, Special Publications*, *42*(1), 313–345.

Tomkins, H., Powell, R., & Ellis, D. (2007). The pressure dependence of the zirconium-in-rutile thermometer. *Journal of Metamorphic Geology*, *25*(6), 703–713.

Triebold, S., von Eynatten, H., & Zack, T. (2012). A recipe for the use of rutile in sedimentary provenance analysis. *Sedimentary Geology*, *282*, 268–275.

Wan, X. (1987). The middle/lower Jurassic of Anqing. *Journal of Stratigraphy*, *11*(3), 187–193. https://doi.org/10.19839/j.cnki.dcxzz.1987.03.004

Wang, P. (1993). Nonmarine fossil bivalves from Wuchang formation, southeastern Hubei, China. *Acta Palaeontologica Sinca*, *32*(6), 725–739.

Wang, X., Liou, J., & Mao, H. (1989). Coesite-bearing eclogite from the Dabie Mountains in Central China. *Geology*, *17*(12), 1085–1088.

Wang, Y., Bai, Q., Ma, W., Yang, J., & Li, Z. (2023). The mid-cretaceous Tectonothermal evolution of the Zhangbaling Tectonic Belt, East China: Evidence from zircon (U–Th)/He and detrital zircon U–Pb dating. *Minerals*, *13*(9), 1–17. https://doi.org/10.3390/min13091142

Wang, Y., Bai, Q., Tian, Z., & Du, H. (2020). Detrital zircon U—Pb dating in the southern Hefei Basin: Evidence for exhumation of HP-UHP rocks of the Dabie Orogen. *Science China Earth Sciences*, *63*, 954–968.

Wang, Y., Bai, Q., Tian, Z., & Du, H. (2021). Mesozoic Unroofing history of the Dabie Orogen, eastern China: Evidence from detrital zircon geochronology of sediments in the Hefei Basin. *The Journal of Geology*, *129*(2), 183–206. https://doi.org/10.1086/714176

Wang, Y., Tian, Z., Hu, Z., & Bai, Q. (2019). Provenance analysis of the Yuantongshan formation in the Hefei Basin and its geological signature: Evidences from detrital zircon dating. *Earth Science Frontiers*, *26*(2), 179–193.

Wang, Y., Zhao, G., Xia, X., Zhang, Y., Fan, W., Li, C., Bi, X., & Li, S. (2009). Early Mesozoic unroofing pattern of the Dabie Mountains (China): Constraints from the U—Pb detrital zircon geochronology and Si-in-white mica analysis of synorogenic sediments in the Jianghan Basin. *Chemical Geology*, *266*(3–4), 231–241.

Wiedenbeck, M., Alle, P., Corfu, F., Griffin, W. L., Meier, M., Oberli, F. V., Quadt, A. V., Roddick, J. C., & Spiegel, W. (1995). Three natural zircon standards for U-Th-Pb, Lu-Hf, trace element and REE analyses. *Geostandards Newsletter*, *19*(1), 1–23.

Willan, R. C. (2003). Provenance of Triassic-cretaceous sandstones in the Antarctic peninsula: Implications for terrane models during Gondwana breakup. *Journal of Sedimentary Research*, *73*(6), 1062–1077.

Wu, Y., & Zheng, Y. (2004). Genesis of zircon and its constraints on interpretation of U—Pb age. *Chinese Science Bulletin*, *49*, 1554–1569.

Wu, Y. B., & Zheng, Y. F. (2013). Tectonic evolution of a composite collision orogen: An overview on the Qinling–Tongbai–Hong'an–Dabie–Sulu orogenic belt in Central China. *Gondwana Research*, *23*(4), 1402–1428.

Wu, Y. B., Zheng, Y. F., Zhao, Z. F., Gong, B., Liu, X., & Wu, F. Y. (2006). U–Pb, Hf and O isotope evidence for two episodes of fluid-assisted zircon growth in marble-hosted eclogites from the Dabie orogen. *Geochimica et Cosmochimica Acta*, *70*(14), 3743–3761.

Wu, Z., Yang, Y., Liu, Y., & Zhang, C. (2023). Detrital zircon geochronology and provenance of metasedimentary rocks from the Susong complex zone in the Dabie Orogen. *Acta Geologica Sinica-English Edition*, *97*, 1335–1354. https://doi.org/10.1111/1755-6724.15073

Xia, M., Zhang, Q. Q., & Gao, X. Y. (2023). Thermal structure of the paleo-continental subduction zone: Insights from quantitatively constrained prograde P–T paths of exhumed LT/UHP eclogites in the Dabie orogen. *Geochemistry, Geophysics, Geosystems*, *24*, e2022GC010852. https://doi.org/10.1029/2022GC010852

Xiong, B. Q. (2016). *SIMS U-Pb geochronology of zircons and rutiles from the South Dabie metamorphic rocks and their tectonic implication, (Doctoral dissertation)* (pp. 1–75). Jilin: Jilin University.

Xiao, Y., Sun, W., Hoefs, J., Simon, K., Zhang, Z., Li, S., & Hofmann, A. W. (2006). Making continental crust through slab melting: Constraints from niobium–tantalum fractionation in UHP metamorphic rutile. *Geochimica et Cosmochimica Acta*, *70*(18), 4770–4782.

Xu, S., Wen, S., Yican, L., Laili, J., Shouyuan, J., Okay, A., & Sengör, A. (1992). Diamond from the Dabie Shan metamorphic rocks and its implication for tectonic setting. *Science*, *256*(5053), 80–82.

Xu, X., & Wang, Q. (2019). The Hualiangting-Mituo ductile shear zone in the Dabie Mountains: Implications for oblique and differential exhumation of ultrahigh-pressure metamorphic slices. *Geological Journal of China Universities*, *25*(2), 182–196.

Yang, J., Cawood, P. A., & Du, Y. (2010). Detrital record of mountain building: Provenance of Jurassic foreland basin to the Dabie Mountains. *Tectonics*, *29*(4), TC4011. https://doi.org/10.1029/2009TC002600

Yang, J., Du, Y., Qin, Y., & Bai, X. (2009). Detrital composition of lower-middle Jurassic sandstones from Huangshi, Hubei: Implication for provenance types and geotectonics. *Journal of Earth Science*, *20*(5), 784–796.

Yang, J., Wang, Y., Bai, Q., & Ma, W. (2022). LA-ICP-MS detrital zircon U-Pb dating of Mesozoic-Cenozoic sedimentary rocks in the Central Hefei Basin and its geological significance. *Advances in Earth Science*, *37*(8), 1–10. https://doi.org/10.11867/j.issn.1001-8166.2022.051

Ye, K., Cong, B., & Ye, D. (2000). The possible subduction of continental material to depths greater than 200 km. *Nature*, *407*(6805), 734–736.

Ye, K., Yao, Y., Katayama, I., Cong, B., Wang, Q., & Maruyama, S. (2000). Large areal extent of ultrahigh-pressure metamorphism

in the Sulu ultrahigh-pressure terrane of East China: New implications from coesite and omphacite inclusions in zircon of granitic gneiss. *Lithos*, *52*(1–4), 157–164.

Yu, J. H., O'Reilly, S. Y., Wang, L., Griffin, W., Zhou, M. F., Zhang, M., & Shu, L. (2010). Components and episodic growth of Precambrian crust in the Cathaysia block, South China: Evidence from U–Pb ages and Hf isotopes of zircons in Neoproterozoic sediments. *Precambrian Research*, *181*(1–4), 97–114.

Yu, J. H., Wang, L., O'reilly, S., Griffin, W., Zhang, M., Li, C., & Shu, L. (2009). A Paleoproterozoic orogeny recorded in a long-lived cratonic remnant (Wuyishan terrane), eastern Cathaysia block, China. *Precambrian Research*, *174*(3–4), 347–363.

Yu, J. J., Chen, Z. Y., Wang, P. A., Li, X. F., Huang, J. P., & Wang, F. (2006). Trace elements geochemistry of rutile in eclogites in the northern Jiangsu province, eastern China. *Acta Petrologica Sinica*, *22*, 1883–1890.

Yu, J. J., Xu, J., Chen, Z. Y., Wang, D. H., Chen, Y. C., Wang, P. A., & Li, X. F. (2006). Trace elements geochemistry of rutile in eclogites from the Chinese continental scientific drilling project main hole. *Acta Geologica Sinica*, *80*, 1835–1841.

Zack, T., & Kooijman, E. (2017). Petrology and geochronology of rutile. *Reviews in Mineralogy and Geochemistry*, *83*(1), 443–467.

Zack, T., Stockli, D. F., Luvizotto, G. L., Barth, M. G., Belousova, E., Wolfe, M. R., & Hinton, R. W. (2011). In situ U–Pb rutile dating by LA-ICP-MS: 208Pb correction and prospects for geological applications. *Contributions to Mineralogy and Petrology*, *162*, 515–530.

Zhang, L., Wang, C., Cao, K., Wang, Q., Tan, J., & Gao, Y. (2016). High elevation of Jiaolai Basin during the late cretaceous: Implication for the coastal mountains along the east Asian margin. *Earth and Planetary Science Letters*, *456*, 112–123.

Zhang, R., Liou, J., & Ernst, W. (2009). The Dabie–Sulu continental collision zone: A comprehensive review. *Gondwana Research*, *16*(1), 1–26.

Zhang, R. J., Meng, F., & Zhang, Z. L. (1982). The Triassic system of southeastern Hubei, China. *Bulletin of Yichang Institute of Geology and Mineral Resources, Chinese Academy of Geological Sciences*, *256*, 39–53.

Zhang, S. B., He, Q., & Zheng, Y. F. (2015). Geochronological and geochemical evidence for the nature of the Dongling complex in South China. *Precambrian Research*, *256*, 17–30.

Zhang, Y., Guo, L., Zhang, H., Harris, N., Xu, W., She, Z., & Luo, T. (2022). Tracing high-pressure metamorphism in the eastern Himalayan syntaxis using detrital zircon and monazite from modern stream sediments. *GSA Bulletin*, *135*(9–10), 2375–2390. https://doi.org/10.1130/B36556.1

Zhang, Y., Shi, Y., Song, C., Li, J., Ren, S., Lin, Z., Qi, F., & Fan, Y. (2017). Sedimentary environments and its geological significance of Jurassic Moshan formation in the northeastern margin of Dabie Mountain. *Acta Petrologica Sinica*, *33*(2), 639–652.

Zhang, Z. M., Shen, K., Sun, W. D., Liu, Y. S., Liou, J., Shi, C., & Wang, J. L. (2008). Fluids in deeply subducted continental crust: Petrology, mineral chemistry and fluid inclusion of UHP metamorphic veins from the Sulu orogen, eastern China. *Geochimica et Cosmochimica Acta*, *72*(13), 3200–3228.

Zhao, G., & Cawood, P. A. (2012). Precambrian geology of China. *Precambrian Research*, *222*, 13–54.

Zhao, L., & Liu, X. (2019). Metallogenic and tectonic implications of detrital zircon U–Pb, Hf isotopes, and detrital rutile geochemistry of late carboniferous karstic bauxite on the southern margin of the North China Craton. *Lithos*, *350*, 105222. https://doi.org/10.1016/j.lithos.2019.105222

Zhao, L., Liu, X., Yang, S., Ma, X., Liu, L., & Sun, X. (2021). Regional multi-sources of carboniferous karstic bauxite deposits in North China craton: Insights from multi-proxy provenance systems. *Sedimentary Geology*, *421*, 105958. https://doi.org/10.1016/j.sedgeo.2021.105958

Zhao, T., Zhu, G., Ye, J., Xu, Z., Xiang, B., Gu, C., Li, Y., Luo, R., Dai, C., & Hu, H. (2022). Interactions between large-scale strike-slip intersecting faults: Implication from the Tan–Lu and Xiangfan–Guangji fault zones in eastern China. *International Geology Review*, *64*(21), 3028–3052. https://doi.org/10.1080/00206814.2021.2010135

Zheng, H., Clift, P. D., He, M., Bian, Z., Liu, G., Liu, X., Xia, L., Yang, Q., & Jourdan, F. (2021). Formation of the first bend in the late Eocene gave birth to the modern Yangtze River. *China Geology*, *49*(1), 35–39.

Zheng, H., Clift, P. D., Wang, P., Tada, R., Jia, J., He, M., & Jourdan, F. (2013). Pre-miocene birth of the Yangtze River. *Proceedings of the National Academy of Sciences*, *110*(19), 7556–7561.

Zheng, Y. (2008). A perspective view on ultrahigh-pressure metamorphism and continental collision in the Dabie-Sulu orogenic belt. *Chinese Science Bulletin*, *53*(20), 3081–3104.

Zheng, Y. F., Fu, B., Gong, B., & Li, L. (2003). Stable isotope geochemistry of ultrahigh pressure metamorphic rocks from the Dabie–Sulu orogen in China: Implications for geodynamics and fluid regime. *Earth-Science Reviews*, *62*(1–2), 105–161.

Zheng, Y. F., Gao, X. Y., Chen, R. X., & Gao, T. (2011). Zr-in-rutile thermometry of eclogite in the Dabie orogen: Constraints on rutile growth during continental subduction-zone metamorphism. *Journal of Asian Earth Sciences*, *40*(2), 427–451.

Zheng, Y. F., Zhao, Z. F., & Chen, R. X. (2019). Ultrahigh-pressure metamorphic rocks in the Dabie–Sulu orogenic belt: Compositional inheritance and metamorphic modification. *Geological Society, London, Special Publications*, *474*(1), 89–132.

Zheng, Y. F., Zhou, J. B., Wu, Y. B., & Xie, Z. (2005). Low-grade metamorphic rocks in the Dabie-Sulu orogenic belt: A passive-margin accretionary wedge deformed during continent subduction. *International Geology Review*, *47*(8), 851–871.

Zhu, G., Liu, G. S., Niu, M. L., Xie, C. L., Wang, Y. S., & Xiang, B. (2009). Syn-collisional transform faulting of the Tan-Lu fault zone, East China. *International Journal of Earth Sciences*, *98*(1), 135–155. https://doi.org/10.1007/s00531-007-0225-8

Zhu, G., Wang, Y., Wang, D., Niu, M., Liu, G., & Xie, C. (2006). Constraints of foreland sedimentation and deformation on synorogenic motion of the Tan-Lu fault zone. *Chinese Journal of Geology*, *41*(1), 102–121.

Zhu, G., Wang, Y., Wang, W., Zhang, S., Liu, C., Gu, C., & Li, Y. (2017). An accreted micro-continent in the north of the Dabie Orogen, East China: Evidence from detrital zircon dating. *Tectonophysics*, *698*, 47–64.

Zhu, G., Xie, C., Xiang, B., Hu, Z., Wang, Y., & Li, X. (2007). Genesis of the Hongzhen metamorphic core complex and its tectonic implications. *Science in China Series D: Earth Sciences*, *50*(5), 649–659.

Zhu, G., Xie, C. L., Chen, W., Xiang, B. W., & Hu, Z. Q. (2010). Evolution of the Hongzhen metamorphic core complex:

Evidence for early cretaceous extension in the eastern Yangtze craton, eastern China. *GSA Bulletin*, *122*(3–4), 506–516.

Zhu, K., Liang, J., Shen, J., Sun, W., & Zhao, J. (2017). Geochemical significance of silicon-bearing rutile in eclogites from Dadie-Sulu ultrahigh pressure metamorphic terrane. *Earth Science Frontiers*, *24*, 288–300.

SUPPORTING INFORMATION

Additional supporting information can be found online in the Supporting Information section at the end of this article.

How to cite this article: Deng, T., Hu, X., Chew, D., Schönig, J., Ma, A., Liang, W., & Drakou, F. (2024). Early Jurassic initiation of the modern drainage pattern of the Dabie orogen (East China) revealed by a multi-proxy provenance approach. *Basin Research*, *36*, e12834. https://doi.org/10.1111/bre.12834